



1 Long-Range Transport Mechanisms in East and Southeast Asia and Impacts on Size-Resolved
2 Aerosol Composition: Contrasting High and Low Aerosol Loading Events

3

4

5 Rachel A. Braun¹, Mojtaba Azadi Aghdam¹, Paola Angela Bañaga^{2,3}, Grace Betito³, Maria
6 Obiminda Cambaliza^{2,3}, Melliza Templonuevo Cruz^{2,4}, Genevieve Rose Lorenzo², Alexander B.
7 MacDonald¹, James Bernard Simpas^{2,3}, Connor Stahl¹, Armin Sorooshian^{1,5}

8

9

10 ¹Department of Chemical and Environmental Engineering, University of Arizona, Tucson, AZ,
11 USA

12 ²Manila Observatory, Loyola Heights, Quezon City 1108, Philippines

13 ³Department of Physics, School of Science and Engineering, Ateneo de Manila University,
14 Loyola Heights, Quezon City 1108, Philippines

15 ⁴Institute of Environmental Science and Meteorology, University of the Philippines, Diliman,
16 Quezon City 1101, Philippines

17 ⁵Department of Hydrology and Atmospheric Sciences, University of Arizona, Tucson, AZ, USA

18

19 Correspondence to: Armin Sorooshian (armin@email.arizona.edu)



20 **Abstract**

21 This study analyzes mechanisms of long-range transport of aerosol and aerosol chemical
22 characteristics in and around East and Southeast Asia. Ground-based size-resolved aerosol
23 measurements collected at the Manila Observatory in Metro Manila, Philippines from July -
24 October 2018 were used to identify and contrast high and low aerosol loading events. Multiple
25 data sources, including models, remote-sensing, and in situ measurements, are used to analyze
26 the impacts of long-range aerosol transport on Metro Manila and the conditions at the local and
27 synoptic scales facilitating this transport. Evidence of long-range transport of biomass burning
28 aerosol from the Maritime Continent was identified through model results and the presence of
29 biomass burning tracers (e.g. K, Rb) in the ground-based measurements. The impacts of
30 emissions transported from continental East Asia are also identified; for one of the events
31 analyzed, this transport was facilitated by the nearby passage of a typhoon. Changes in the
32 aerosol size distributions, water-soluble chemical composition, and contributions of various
33 organic aerosol species to the total water-soluble organic aerosol were examined for the different
34 cases. The events impacted by biomass burning transport had the overall highest concentration of
35 water-soluble organic acids, while the events impacted by long-range transport from continental
36 East Asia, showed high percent contributions from shorter chain dicarboxylic acids (i.e. oxalate)
37 that are often representative of photochemical and aqueous processing in the atmosphere. The
38 low aerosol loading event was subject to a larger precipitation accumulation than the high
39 aerosol events, indicative of wet scavenging as an aerosol sink in the study region. This low
40 aerosol event was characterized by a larger relative contribution from supermicrometer aerosols
41 and had a higher percent contribution from longer-chain dicarboxylic acids (i.e. maleate) to the
42 water-soluble organic aerosol fraction. Results of this study have implications for better
43 understanding of the transport and chemical characteristics of aerosol in a highly-populated
44 region that has thus far been difficult to measure through remote-sensing methods. Furthermore,
45 findings associated with the effects of air mass mixing on aerosol physiochemical properties are
46 applicable to other global regions impacted by both natural and anthropogenic sources.
47



48 1. Introduction

49 Better understanding of long-range transport of aerosol is critical for determining the fate
50 of atmospheric emissions and improving models of atmospheric aerosol. Nutrients (e.g. Duce et
51 al., 1991; Artaxo et al., 1994), bacteria (e.g. Bovallius et al., 1978; Maki et al., 2019), and
52 pollutants (e.g. Nordø, 1976; Lyons et al., 1978; Lindqvist et al., 1991) can be transported
53 through the atmosphere over large distances across the globe. Atmospheric aerosol can undergo
54 physiochemical changes through photochemical and aqueous-processing mechanisms such that
55 their characteristics at the emission source can be quite different from those farther downwind
56 (e.g. Yokelson et al., 2009; Akagi et al., 2012). Large uncertainties remain in atmospheric
57 aerosol models due to impacts of aqueous processing and wet scavenging on aerosol (Kristiansen
58 et al., 2016; Xu et al., 2019). Although impacts and processes of long-range aerosol transport
59 have worldwide applicability, the strong facilitation of transport by synoptic scale conditions
60 necessitates detailed analyses of transport events at the regional level.

61 Both natural and anthropogenic emissions contribute to atmospheric aerosol worldwide.
62 However, the plethora of both types of sources in and around the Southeast (SE) Asia, the
63 proximity of islands and continental regions in SE and East Asia, and the large, growing
64 population makes SE Asia a prime candidate for the study of long-range transport of atmospheric
65 aerosol. Moreover, the extensive cloud coverage and precipitation during certain times of the
66 year in SE Asia allow for an examination of the effects of aqueous processing and wet
67 scavenging. Characterizations of aerosol in mainland SE Asia and the Maritime Continent (MC),
68 which includes the islands south of the Philippines and north of Australia (e.g. islands part of
69 Malaysia and Indonesia), have found major emission sources to be industrial activities, shipping,
70 urban mega-cities, and biomass burning (Reid et al., 2013). In addition, natural emission sources,
71 including marine emissions, plant life, and occasionally volcanic eruptions, intermingle with
72 anthropogenic emissions. Mixing of aerosol from anthropogenic and biogenic sources has been
73 noted to be influential in the overall production of secondarily produced aerosol via gas-to-
74 particle conversion processes (Weber et al., 2007; Goldstein et al., 2009; Brito et al., 2018). In
75 addition, the mixing of marine and biomass burning emissions can produce compositional
76 changes, such as enhancements in chloride depletion (e.g. Braun et al., 2017) and
77 methanesulfonate (MSA) production (Sorooshian et al., 2015). The mechanisms governing
78 aerosol changes in mixed air masses have wide-ranging and complex impacts and require further
79 study in regions, such as SE Asia, that are impacted by multiple aerosol emission sources.

80 One major contributor to atmospheric aerosol in SE Asia and the MC that has received
81 considerable attention is biomass burning. Biomass burning in SE Asia appears to be dominated
82 by anthropogenic activities, such as peatland burning (Graf et al., 2009; Reid et al., 2013; Latif et
83 al., 2018) and rice straw open field burning (Gadde et al., 2009). However, current satellite
84 retrievals underestimate the true emissions in the region (Reid et al., 2013). Identification of
85 biomass burning emissions in the MC using satellite-based observations is difficult for numerous
86 reasons, including the characteristics of fires common to the region (e.g. low-temperature peat-
87 burning) and abundant cloud cover (Reid et al., 2012, 2013). However, the potential for long-
88 range transport of biomass burning emissions from the MC has received considerable attention
89 (Wang et al., 2013; Xian et al., 2013; Reid et al., 2016a; Atwood et al., 2017; Ge et al., 2017;
90 Song et al., 2018). In order to better understand the prevalence and fate of biomass burning
91 emissions in the MC and SE Asia, both in situ measurements and modeling studies are needed.
92 Insights into the fate of biomass burning emissions in the atmosphere are crucial and applicable



93 on a global scale, especially since studies have indicated an increasing trend in biomass burning
94 worldwide (Flannigan et al., 2009, 2013).

95 As a mega-city in SE Asia, Metro Manila, Philippines (Population ~12.88 million;
96 Philippine Statistics Authority, 2015) is a prime location for the study of locally-produced urban
97 anthropogenic aerosol (Kim Oanh et al., 2006) that is mixed with biogenic, natural, and
98 anthropogenic pollutants from upwind areas. Previous research conducted at the Manila
99 Observatory (MO) in Quezon City, Metro Manila characterized seasonal trends in PM_{2.5}
100 (particulate matter (PM) with aerodynamic diameter less than 2.5 μm) and sources of measured
101 particles, with traffic emissions being the major source at MO (Simpas et al., 2014). Additional
102 studies have further characterized vehicular emissions by focusing on black carbon (BC)
103 particulate concentrations in sites around the Metro Manila region, including near roadways
104 (Bautista et al., 2014; Kecorius et al., 2017; Alas et al., 2018). Due to very high population
105 density in Metro Manila, it is expected that many of the urban PM sampling sites are highly
106 affected by local anthropogenic sources as opposed to long-range transport. However, the
107 proximity of the Philippines to other islands and continental Asia raises the question of the
108 relative impacts of long-range transport as opposed to local emissions on not just Metro Manila,
109 but also downwind regions.

110 Long-range transport to the Philippines varies by season since there is a strong change in
111 weather patterns throughout the year (Bagtasa et al., 2018). Another study of the aerosol over the
112 South China Sea (SCS), which is bordered to the east by the Philippines, found seasonal changes
113 in aerosol emission sources, with year-round anthropogenic pollution, smoke from the MC
114 between August – October, and dust from northern continental Asia between February – April
115 (Lin et al., 2007). The season from approximately June – September (Cayanan et al., 2011; Cruz
116 et al., 2013), referred to as the Southwest Monsoon (SWM) season, is characterized by increased
117 prevalence of southwesterly winds and precipitation. During the SWM season, biomass burning
118 is prevalent in the MC, while biomass burning is more common in continental SE Asia during
119 the winter and spring (Lin et al., 2009; Reid et al., 2013). During the northeast monsoon, aerosol
120 influences from northern East Asia were measured in the northwestern edge of the Philippines
121 (Bagtasa et al., 2018). In addition to transport of aerosol to the Philippines, the influence of
122 emission outflows from the Philippines has also been measured in the northern SCS at Dongsha
123 Island (Chuang et al., 2013) and in coastal southeast China (Zhang et al., 2012). Long-range
124 transported aerosol in SE and East Asia have various sources, and therefore, different
125 physiochemical properties. However, the prevalence of the signal of long-range transported
126 aerosol in a highly polluted mega-city, such as Metro Manila, is not well characterized.

127 As recent studies have indicated a decline in SWM rainfall in the western Philippines and
128 an increase in no-rain days during the typical SWM season (Cruz et al., 2013), the potential for
129 wet scavenging of aerosol during these time periods could be decreasing. Furthermore, decreases
130 in monsoonal rainfall in other parts of Asia, including India (Dave et al., 2017) and China (Liu et
131 al., 2019), have been linked to increases in aerosol, especially those of anthropogenic origin.
132 Reinforcing mechanisms in these interactions, such as decreased rainfall reducing wet
133 scavenging, leading to higher aerosol concentrations that in turn suppress precipitation, and the
134 corresponding climatic changes in monsoonal rain in the western Philippines underscore the need
135 to better understand the processes governing atmospheric aerosol characteristics and sources,
136 especially during the monsoonal season.

137 The present study focuses on three high-aerosol loading events, contrasted with a very
138 low aerosol event, as identified by ground-based observations collected at MO from July -



139 October 2018. The objectives of the study are to (i) describe synoptic and local scale conditions
140 facilitating various transport cases, (ii) isolate characteristic aerosol physiochemical properties
141 indicative of long-range transport, and (iii) identify transformational processes, especially with
142 regard to chemical composition, of aerosol during long-range transport to the highly-populated
143 Metro Manila region. The results of this work have implications for better understanding of (i)
144 the fate of biomass burning emissions in a region with prevalent wildfires that are poorly
145 characterized by remote-sensing, (ii) the impact of transformational and removal mechanisms,
146 including aqueous processing, photochemical reactions, and wet scavenging, on long-range
147 transported aerosol from multiple sources, and (iii) typical synoptic and local scale behavior of
148 aerosol in a region that is both highly populated and gaining increasing attention due to
149 campaigns such as the NASA-sponsored Clouds, Aerosols, and Monsoon Processes Philippines
150 Experiment (CAMP²Ex).

151

152 **2. Methodology**

153 **2.1 Ground-Based Observations**

154 As part of a year-long sampling campaign (CAMP²Ex weathER and CompoSition
155 Monitoring: CHECSM) at the Manila Observatory (MO; 14.64° N, 121.08° E) in Quezon City,
156 Metro Manila, Philippines, 12 sets of size-resolved aerosol were collected from July - October
157 2018 using a Micro-Orifice Uniform Deposit Impactor (MOUDI; Marple et al., 2014). Details
158 for the 12 size-resolved sets can be found in Table 1. Sample Teflon substrates (PTFE
159 membrane, 2 μm pore, 46.2 mm diameter, Whatman) were cut in half for preservation for future
160 analysis. Half-substrates were extracted in 8 mL of Milli-Q water (18.2 MΩ-cm) in sealed
161 polypropylene vials through sonication for 30 min. Aqueous extracts were subsequently analyzed
162 for ions using ion chromatography (IC; Thermo Scientific Dionex ICS-2100 system) and
163 elements using triple quadrupole inductively coupled plasma mass spectrometry (ICP-QQQ;
164 Agilent 8800 Series). The list of analyzed species and limits of detection for those species can be
165 found in Table S1, with limits of detection in the ppt range for ICP and the ppb range for IC.
166 Background concentrations were also subtracted from each sample. For each MOUDI set
167 (naming convention: MO#), the mass concentration sum of the water-soluble species was
168 calculated; using this summation, the three high-aerosol loading events were identified (MO7,
169 MO12, and MO14), as well as the lowest aerosol event (MO11).

170

171 **2.2 Remote-Sensing Observations**

172 Retrievals of atmospheric profiles from the Cloud-Aerosol Lidar with Orthogonal
173 Polarization (CALIOP) onboard the Cloud-Aerosol Lidar and Infrared Pathfinder Satellite
174 Observations (CALIPSO) were taken for select satellite overpasses corresponding to MOUDI
175 sample sets of interest (Winker et al., 2009). Previous studies have examined the ability of
176 CALIOP to capture atmospheric profiles in SE Asia and the MC, with one major challenge in
177 this region being the lack of cloud-free schemes (Campbell et al., 2013; Ross et al., 2018).
178 Overpasses corresponding to the three highest aerosol events were analyzed, but no data was
179 available for the time encompassing MO11. The CALIOP Level 2 Vertical Feature Mask (VFM)
180 was used to distinguish between clear air, clouds, and aerosol (Vaughan et al., 2004).

181

182 **2.3 Models**

183 To describe the synoptic scale conditions, data were used from the Modern-Era
184 Retrospective analysis for Research and Applications, Version 2 (MERRA-2; Gelaro et al.,



185 2017). Horizontal winds at 850 hPa (GMAO, 2015a) were temporally averaged over the
186 sampling period using 3-hourly instantaneous data and subsequently spatially averaged to
187 increase figure readability. The total cloud area fraction (GMAO, 2015b) was also temporally
188 averaged over the sampling period using 1-hourly time-averaged MERRA-2 data.

189 Five-day air mass back-trajectories were calculated using the Hybrid Single Particle
190 Lagrangian Integrated Trajectory (HYSPLIT) model from NOAA (Stein et al., 2015) and
191 gridded meteorological data from the National Centers for Environmental Prediction/National
192 Center for Atmospheric Research (NCEP/NCAR) reanalysis project. The model was run for
193 back-trajectories terminating at the MOUDI inlet (~85 m above sea level) every 6 h during each
194 sample set. The HYSPLIT model has been used extensively in studies focused on regions across
195 the globe to study aerosol transport (Stein et al., 2015).

196 Precipitation amounts were found using the Precipitation Estimation from Remotely
197 Sensed Information using Artificial Neural Networks—Cloud Classification System
198 (PERSIANN-CCS) dataset (Hong et al., 2004), which is available from the UC Irvine Center for
199 Hydrometeorology and Remote Sensing (CHRS) Data Portal (<http://chrsdata.eng.uci.edu>,
200 Nguyen et al., 2019). PERSIANN-CCS has previously been used to analyze precipitation events
201 in the region of interest, as shown by the successful characterization of rainfall during Typhoon
202 Haiyan over the Philippines in November 2013 (Nguyen et al., 2014). Precipitation accumulated
203 during the sample sets (Table 1) was calculated to be the average found for the region
204 surrounding MO in the box bounded by 121.0199 - 121.0968° E and 14.6067 - 14.6946° N.

205 To further describe long-range transport activity, results from the Navy Aerosol Analysis
206 and Prediction System (NAAPS) operational model are included for the selected study periods
207 (Lynch et al., 2016; <https://www.nrlmry.navy.mil/aerosol/>). Global meteorological fields used in the
208 NAAPS model are supplied by the Navy Global Environmental Model (NAVGEM; Hogan et al.,
209 2014). The NAAPS model has previously been employed to study aerosol in the MC (e.g. Xian
210 et al., 2013).

211

212

3. Results

213

3.1 Cases of Long-Range Aerosol Transport

214

215 The following sub-sections (3.1.1-3.1.4) describe the synoptic and local scale
216 meteorological conditions governing long-range aerosol transport during the three highest
217 aerosol events (MO7, MO12, and MO14) and, for the purposes of comparison, the lowest aerosol
218 event (MO11). Also included are characterizations of aerosol from remote-sensing and model
219 results. Results of size-resolved aerosol characterization at MO are discussed in Section 3.2.

219

220

3.1.1 MO7 (August 14 – 16, 2018): Smoke Transport from Maritime Continent

221

222 Many previous studies have focused on the prevalence of biomass burning in the MC and
223 the potential for transport of smoke towards the Philippines (Wang et al., 2013; Xian et al., 2013;
224 Reid et al., 2016a; Atwood et al., 2017; Ge et al., 2017; Song et al., 2018). Figure 1a shows the
225 average 850 hPa wind vectors and cloud fraction for the MO7 sampling period. The prevailing
226 wind direction was towards the northeast, consistent with typical SWM flow. Furthermore, areas
227 with lower cloud coverage were present to the southwest of Metro Manila. The HYSPLIT back-
228 trajectory for this sample set also shows an air mass originating around the MC to the southwest
229 of MO that is then transported over the ocean towards the Philippines (Figure 2a). As evidenced
230 by the name of the season (i.e. Southwest Monsoon), this trajectory is typical for this time of the
year and was the dominating trajectory pattern for the remaining eight sample sets not chosen for



231 in-depth analysis (Figure S1). Furthermore, for MO1 – MO10 (i.e. all sample sets with prevailing
232 southwesterly wind influence), MO7 had the lowest rain amount for the surrounding region,
233 followed by MO8, which had the 4th highest water-soluble aerosol concentration (Table 1). This
234 suggests that wet scavenging could have been less influential in MO7 and MO8, thereby leading
235 to an increase in the PM measured. Three CALIPSO overpasses near MO occurred during the
236 MO7 sample set and one occurred during the nighttime after sampling ended; however, the
237 signal was largely attenuated in the lower 8 km during the daytime samples for the area
238 surrounding MO (Figure S2). In the case of the two nighttime overpasses (Figure 3), which
239 sampled to the southwest of Manila, a deep aerosol layer is observed in the VFM extending from
240 the surface to around 3 km (Figure 3). This classic case of long-range transport from the MC to
241 the Philippines during the SWM season is also clearly shown in the biomass burning smoke
242 surface concentrations from the NAAPS model (Figure 4a).

243

244 **3.1.2 MO11 (September 18 – 20, 2018): Lowest Aerosol Event**

245 MO11 had the lowest overall water-soluble aerosol mass concentration ($2.7 \mu\text{g m}^{-3}$),
246 which is over six times lower than the highest aerosol MOUDI set. As evidenced by both the 850
247 hPa wind vectors (Figure 1b) and the HYSPLIT back-trajectories (Figure 2b) from this set,
248 conditions are very different from the highest three aerosol events and show transport patterns
249 with flow originating over the open ocean to the east of the Philippines moving almost due west.
250 The lack of anthropogenic aerosol sources in the path of the back-trajectories could result in the
251 overall low amount of aerosol observed. This set was also characterized by high accumulated
252 rainfall amounts for the region in the path of the back-trajectories (Figure 2b) and in the area
253 surrounding MO as compared to the highest aerosol events (Table 1), increasing the possibility
254 that wet scavenging effectively removed most of the transported (and, to some extent, local)
255 aerosol. In addition, the NAAPS model showed no smoke influence from the MC and an isolated
256 anthropogenic and biogenic fine aerosol plume around Metro Manila, suggesting local sources
257 accounted for the majority of the measured aerosol (Figure 4b).

258

259 **3.1.3 MO12 (September 26 – 28, 2018): Impacts of Typhoon Trami**

260 Typhoon Trami (Category 5) passed to the northeast of the island of Luzon in the
261 Philippines during MO12 (Figure 1c). Typhoon influences on atmospheric aerosol, caused by
262 varying factors such as wind speed and precipitation, have been studied in China (Yan et al.,
263 2016; Liu et al., 2018), Korea (Kim et al., 2007), Malaysia (Juneng et al., 2011), the South China
264 Sea (Reid et al., 2015, 2016b), and Taiwan (Fang et al., 2009; Chang et al., 2011; Lu et al.,
265 2017). The influences of typhoons on biomass burning emissions and transport in the MC have
266 also been examined (Reid et al., 2012; Wang et al., 2013). In this case, the influence of this storm
267 changed the prevailing wind direction approaching the northern Philippines, effectively pulling
268 an air mass from the west of the island, and along with it, emissions from continental East Asia
269 (Figure 2c). Furthermore, the air mass passed through regions of relatively little rainfall during
270 transport to the Philippines (Figure 2c), and accumulated rainfall at MO during this sample set
271 was very low (Table 1). One CALIPSO overpass around the ending time of set MO12 and one
272 during the nighttime after sampling ended (Figure 3) show that in the direction of transport (i.e.
273 north of the MO, from around 15–20° N), there is an aerosol layer extending up to around 2 km
274 during the day (northwest of MO) and 3 km at night (northeast of MO). The influence of
275 emissions from continental East Asia is also apparent in the NAAPS model (Figure 4c).
276 Observations at Dongsha Island, located to the north of the Philippines, have revealed influence



277 from Gobi Desert emissions (Wang et al., 2011) and anthropogenic sources (Atwood et al.,
278 2013). Farther south in the MC, aerosol measurements in Malaysia have also indicated influence
279 of aged, long-range transport from sites to the north in East Asia (Farren et al., 2019).

280

281 **3.1.4 MO14 (October 6 – 8, 2018): Mixed Influences**

282 The final MOUDI set (MO14) included in this study represents a transition in
283 meteorological regimes at the end of the SWM season and resulted in the highest overall water-
284 soluble mass concentration. This event had some of the lowest rainfall amounts in the region
285 surrounding Metro Manila (Figure 2d), with zero accumulated precipitation at MO during the
286 sampling period (Table 1). Furthermore, low cloud fraction was observed for regions to the
287 northwest and east of Metro Manila (Figure 1d). Back-trajectories from HYSPLIT show that the
288 air mass appeared to be influenced by a mix of continental sources in East Asia and local sources
289 (Figure 2d). Furthermore, two CALIPSO overpasses, one during the nighttime while sampling
290 was occurring and the other during the daytime after sampling ended, show a deep aerosol layer
291 north of MO, extending from the surface to around 2 km on October 6th and lower on October 8th
292 (Figure 3). From the NAAPS model, it appears that a mixture of MC smoke emissions and
293 continental East Asia emissions converge around the northern Philippines (Figure 4d).

294

295 **3.2. Ground-Based Aerosol Chemical Composition**

296 **3.2.1 Size-Resolved Aerosol Characteristics**

297 The water-soluble mass size distributions and the percent contribution of each MOUDI
298 stage to the water-soluble mass for the four sets of interest (MO7, MO12, MO14, and MO11)
299 and the average (\pm one standard deviation) of the remaining sets (MO1 – MO6, MO8 – MO10)
300 are shown in Figure 5. Most of the sets show a bimodal distribution with peaks in both the
301 submicrometer and supermicrometer range; one exception is the lowest aerosol event (MO11),
302 which shows a fairly broad size distribution. The highest aerosol event, MO14, shows a
303 significant peak in the submicrometer range, with a very large drop in mass concentration in the
304 supermicrometer range. This is in stark contrast to the lowest aerosol event (MO11), which
305 shows that the supermicrometer range contributes the greatest percent to the total water-soluble
306 mass. The second and third highest aerosol events, MO7 and MO12, also show significant
307 enhancements in the supermicrometer range as compared to the average of the other sets and
308 MO14.

309 Examination of the major species contributing to the water-soluble mass (Figure 6) can
310 lend additional insights into the variability in the size distributions. MO14 had one of the highest
311 combined contributions of SO_4^{2-} and NH_4^+ (77.2% of water-soluble mass), with only MO10
312 being slightly larger at 77.6%. These two species are typically associated with the submicrometer
313 range and anthropogenic origins due to their formation through secondary processes such as gas-
314 to-particle conversion of gaseous SO_2 and NH_3 , respectively, and aqueous processing to form
315 SO_4^{2-} (Ervens, 2015). In contrast, MO11 had the lowest overall combined percent contribution of
316 these two species (41.4%) to the water-soluble aerosol mass. Of all 12 SWM MOUDI sets,
317 MO11 had the highest percent contributions from Ca^{2+} (14.0%) and Cl^- (12.5%), as well as one
318 of the highest contributions from Na^+ (10.7%). Each of these species is associated with primary
319 emissions, including dust in the case of Ca^{2+} and sea salt for Na^+ and Cl^- , resulting in larger
320 particles (i.e. $> 1 \mu\text{m}$). The HYSPLIT back-trajectories for MO11 match well with the MOUDI
321 results, as the influence of marine aerosol (i.e. Na^+ , Cl^-) and lack of anthropogenic sources of
322 SO_2 and NH_3 is apparent. Local sources of dust most likely contribute the highest amount to the



323 measured Ca^{2+} , as the back-trajectories show few other crustal sources farther upwind. Average
324 size-resolved profiles for all of the species in these 12 sample sets can be found in Cruz et al.
325 (2019), with characteristic size distribution profiles agreeing with the above assessments.
326

327 **3.2.2 Enhancements in Tracer Species**

328 In addition to insights from the major water-soluble chemical species found in aerosol,
329 tracer aerosol species can also be used to identify impacting emission sources (e.g. Fung and
330 Wong, 1995; Allen et al., 2001; Ma et al., 2019). For the aforementioned high aerosol events,
331 numerous tracer species are elevated in some, but not all, sample sets. This makes these species
332 prime candidates for linking influencing sources to the measured ambient aerosol. The authors
333 theorize that MO8, which was the 4th highest aerosol event (Table 1), also was impacted by
334 biomass burning due to the back-trajectory analysis (Figure S1), NAAPS model (Figure S3), and
335 increases in select species described subsequently. Therefore, MO8 was separated from the other
336 sample sets for the purposes of the following characterizations. Figure 7 shows the size-resolved
337 aerosol composition for select tracer species for the four highest aerosol events (MO7, MO8,
338 MO12, and MO14), the lowest aerosol event (MO11), and the average (\pm standard deviation) of
339 the remaining seven sample sets.

340 Potassium is frequently used as a biomass burning tracer (e.g. Andreae, 1983; Artaxo et
341 al., 1994; Echalar et al., 1995; Chow et al., 2004; Thepnuan et al., 2019). This species shows
342 highly elevated levels in the submicrometer range for MO7 and MO8 (i.e. the sets influenced by
343 biomass burning transport from the MC). Other elevated trace elements for these two profiles
344 include Rb, Cs, Se, and Ti (Figure 7). Previous studies in the western United States (Schlosser et
345 al., 2017; Ma et al., 2019) have also shown Rb enhancements in wildfire-influenced aerosol. Rb
346 has also been measured in flaming and smoldering biomass burning emissions (Yamasoe et al.,
347 2000). Enhancements in Rb and Cs in the fine fraction of aerosol influenced by wildfire
348 emissions have been observed in South Africa (Maenhaut et al., 1996), with similar results
349 shown in this study for aerosol in the submicrometer size range. Se is also enhanced for these
350 two sets in the submicrometer range, as it is often formed through gas-to-particle conversion
351 processes of inorganic Se compounds (Wen and Carignan, 2007). A wide variety of sources for
352 atmospheric Se exist (Mosher and Duce, 1987), including, but not limited to, coal combustion
353 (Thurston and Spengler, 1985; Fung and Wong, 1995; Song et al., 2001), marine emissions
354 (Arimoto et al., 1995), volcanos, and biomass burning (Mosher and Duce, 1987). In contrast to
355 the other enhanced species for MO7 and MO8, the mass concentration mode for Ti resides in
356 supermicrometer size range. Ti is typically associated with crustal material that can be suspended
357 through mechanisms such as vehicle usage (Sternbeck et al., 2002; Querol et al., 2008; Amato et
358 al., 2009) and lofting in wildfire plumes (Maudlin et al., 2015; Schlosser et al., 2017). While
359 long-range transport of biomass burning aerosol could lead to the enhancements measured for
360 these biomass burning tracer species, local emission sources, such as waste burning and wood
361 burning for cooking, may also play a role.

362 Two tracer species are included that showed enhancements for MO12, specifically Ba in
363 the supermicrometer range and V in the submicrometer range (Figure 7). One well-documented
364 source of aerosol Ba is non-exhaust vehicle emissions, including brakewear (Sternbeck et al.,
365 2002; Querol et al., 2008; Amato et al., 2009; Jeong et al., 2019). V also has well characterized
366 emission sources, most specifically fuel combustion (Fung and Wong, 1995; Artaxo et al., 1999;
367 Song et al., 2001; Lin et al., 2005; Kim and Hopke, 2008). In coastal environments, V is often
368 tied to shipping emissions (Agrawal et al., 2008; Pandolfi et al., 2011; Maudlin et al., 2015;



369 Mamoudou et al., 2018). As these sources are anthropogenic in origin, it is difficult to determine
370 the relative influences of long-range transport versus local emissions, especially with the
371 proximity of the sampling site to major roadways and shipping in Manila Bay. However, the
372 enhancement in V could result from the transport of the aerosol over major shipping lanes father
373 upwind.

374 Finally, Figure 7 shows three selected elements that appear enhanced in MO14, all of
375 which are typically tied to anthropogenic sources. Both Pb and Sn are found mainly in the
376 submicrometer range and have been linked by previous studies to vehicle emissions (Singh et al.,
377 2002; Amato et al., 2009), industrial emissions (Querol et al., 2008; Allen et al., 2001), and
378 waste burning (Kumar et al., 2015). Other sources of Pb could include E-waste recycling
379 (Fujimori et al., 2012) and biomass burning (Maenhaut et al., 1996). The size distribution of Mo
380 for MO14 shows a much broader distribution, with peaks in both the sub- and supermicrometer
381 ranges. Sources of Mo include vehicle emissions (Pakkanen et al., 2003; Amato et al., 2009),
382 combustion (Pakkanen et al., 2001, 2003), and industrial activity, including copper smelters
383 (Artaxo et al., 1999). As is the case with the enhanced species in MO12, the anthropogenic
384 nature of these species makes it difficult to determine the relative contribution of long-range
385 versus local emissions. However, as both MO12 and MO14 show enhancements in
386 anthropogenic-produced trace elements, the influence of long-range transport from industrial and
387 urban areas in continental East Asia is plausible.

388 3.2.3 Variability of Water-Soluble Organic Species

389 Water-soluble organic aerosol species serve as good tracers for emission sources, impact
390 the cloud condensation nuclei (CCN) budget, and contribute non-negligible mass to atmospheric
391 aerosol. Figure 8 shows the sum of the total measured water-soluble organic species and the
392 relative contributions of oxalate, succinate, adipate, maleate, pyruvate, MSA, and phthalate to the
393 total measured water-soluble organics for MO7, MO8, MO11, MO12, MO14, and the average (\pm
394 one standard deviation) of the remaining sets. Malonate (C3) was not characterized due to its low
395 concentrations in the samples measured and the co-elution of C3 with carbonate in the IC
396 analysis. Glutarate (C5) was also excluded from the analysis due to very low concentrations. For
397 the examination of the organic species, MO8 was again separated from the other MOUDI sets
398 due to it having the second highest concentration of organic species ($0.66 \mu\text{g m}^{-3}$) and an organic
399 species contribution profile very similar to that of MO7. The remaining MOUDI sets included in
400 the average category (MO1 – MO6, MO9 – MO10) all have total organic species concentrations
401 that were less than the four highest aerosol sets (MO7, MO8, MO12, MO14) and greater than the
402 lowest aerosol set (MO11). The lowest aerosol event (MO11) has the lowest overall
403 concentration of organic aerosol ($0.09 \mu\text{g m}^{-3}$), while the 2nd highest aerosol event (MO7) has the
404 highest concentration of organic aerosol ($0.70 \mu\text{g m}^{-3}$).

405 Many studies worldwide have examined the relative contributions of organic species to
406 atmospheric aerosol, with oxalate typically having the highest contribution among dicarboxylic
407 acids (Kawamura and Kaplan, 1987; Kawamura and Ikushima, 1993; Kawamura and Sakaguchi,
408 1999; Sorooshian et al., 2007a; Hsieh et al., 2007, 2008; Aggarwal and Kawamura, 2008;
409 Deshmukh et al., 2012, 2018; Li et al., 2015; Hoque et al., 2017; Kunwar et al., 2019). Oxalate
410 was the dominant water-soluble organic species for all 12 MOUDI sets, with oxalate having the
411 highest contribution to the organic aerosol in MO12 (88.7% of total organic aerosol). Oxalate is
412 often considered a byproduct of photochemical aging of longer-chain dicarboxylic acids (e.g.
413 Kawamura and Ikushima, 1993; Kawamura and Sakaguchi, 1999), and therefore an increase in
414



415 oxalate is often considered a signature of aged aerosol in the absence of primary oxalate
416 emissions from sources such as biomass burning. Another major pathway of oxalate formation is
417 aqueous processing (Crahan et al., 2004; Ervens et al., 2004, 2018; Sorooshian et al., 2006,
418 2007b; Wonaschuetz et al., 2012), which is likely prevalent during the SWM when there is
419 frequent cloud cover. Previous studies have also demonstrated the ability for transport of and
420 photochemical aging of water-soluble organic acids over long distances in a marine environment
421 (e.g. Kawamura and Sakaguchi, 1999) and the importance of emissions from continental Asia in
422 the organic aerosol budget in the western north Pacific (Aggarwal and Kawamura, 2008; Hoque
423 et al., 2017). The back-trajectories of the air masses terminating at MO during MO12 and MO14
424 indicate origins of emissions from continental East Asia (Figure 2). It is plausible that the high
425 contribution of oxalate to the organic aerosol in MO12 and MO14 (which had the fourth highest
426 percent contribution of oxalate) is due to the degradation of both primarily-emitted and
427 secondarily-produced longer-chain dicarboxylic acids during the transport process through
428 mechanisms described above, such as photochemical degradation and aqueous processing, with
429 the former mechanism being plausible in the regions of low cloud cover to the north and
430 northwest of the Manila (Figure 1) and the latter mechanism potentially being of great
431 importance due to the typhoon influences during transport. While the aerosol measured in MO7
432 and MO8 also show long-range transport influences (Figure 2a and Figure S1), the overall signal
433 of organic aerosol is much stronger in these two sets, such that the absolute concentration of
434 oxalate (MO7: $0.47 \mu\text{g m}^{-3}$ and MO8: $0.42 \mu\text{g m}^{-3}$) is still greater than in MO12 ($0.19 \mu\text{g m}^{-3}$)
435 and MO14 ($0.37 \mu\text{g m}^{-3}$). However, biomass burning is a well-documented source of both
436 oxalate and longer-chain dicarboxylic acids (e.g. Falkovich et al., 2005; Nirmalkar et al., 2015;
437 Cheng et al., 2017; Deshmukh et al., 2018; Thepnuan et al., 2019).

438 Succinate has been linked to biomass burning emissions (Wang and Shooter, 2004;
439 Falkovich et al., 2005; Zhao et al., 2014; Balla et al., 2018), vehicular emissions (Kawamura and
440 Kaplan, 1987; Kawamura et al., 1996; Yao et al., 2004), and secondary production via
441 photochemical reactions of precursor organic compounds (Kawamura and Ikushima, 1993;
442 Kawamura et al., 1996; Kawamura and Sakaguchi, 1999). The two MO MOUDI sets thought to
443 have the most influence from biomass burning emissions (MO7 and MO8) had the highest
444 organic aerosol mass concentrations and the highest mass percent contributions of succinate to
445 the organic aerosol (MO7: 14.3% and MO8: 17.5%). In contrast, the next highest contribution of
446 succinate to the organic aerosol was 4.2% measured in MO5. These results agree with previous
447 studies in Northeast China that showed an increase in total organic aerosol mass concentration
448 and a strong increase (decrease) in the relative contribution of succinate (oxalate) during biomass
449 burning periods as opposed to non-biomass burning periods (Cao et al., 2017). Results from
450 California, USA also showed higher percent contributions of succinate to the water-soluble
451 organic aerosol during periods influenced by biomass burning (Maudlin et al., 2015).

452 MO11 had the second highest relative contribution of maleate (28.5% of water-soluble
453 organic aerosol) out of all 12 sample sets and had a much higher percent contribution as
454 compared to the four highest aerosol events ($<2.5\%$ for each of the following: MO7, MO8,
455 MO12, and MO14). Maleate is linked to the oxidation of aromatic hydrocarbons, usually from
456 anthropogenic sources such as vehicular emissions (Kawamura and Kaplan, 1987; Kunwar et al.,
457 2019). One explanation for this result could be the higher rainfall accumulation in and around the
458 study region during MO11 as compared to the three highest aerosol sets (Figure 2). Wet
459 scavenging could have removed aerosol from transported air masses during their journey towards
460 MO, thereby increasing the relative contribution of local sources to the measured aerosol in



461 MO11. Because of the reduced aging time associated with emissions from local sources, the
462 relative increase in the contribution of longer-chain dicarboxylic acids and the decrease in the
463 relative contribution of oxalate is plausible. Hsieh et al. (2008) showed in samples from Taiwan
464 that the relative contribution of oxalate to the organic acids was also higher during periods of
465 high aerosol loading as opposed to periods of moderate aerosol loading when the overall PM
466 concentration was lower. MO11, which showed air mass back-trajectories originating to the east
467 of the Philippines from the open Pacific (Figure 2b), had the lowest overall water-soluble PM
468 concentration, the lowest overall concentration of water-soluble organic acids, and the second
469 lowest percent contribution of oxalate to the organic acid mass (57.1%) of all the sets.

470 Phthalate is an aromatic dicarboxylic acid often linked to anthropogenic sources through
471 photochemical transformation of emissions from vehicles (Kawamura and Kaplan, 1987;
472 Kawamura and Ikushima, 1993) and waste burning (Kumar et al., 2015), although aqueous
473 processing has also been proposed as a formation mechanism (Kunwar et al., 2019).
474 Accordingly, phthalate has been shown to have seasonal and diurnal variations in concentration,
475 with enhanced production usually linked to times of stronger solar radiation (i.e. summertime
476 and daytime: Satsumabayashi et al., 1990; Ray and McDow, 2005; Ho et al., 2006; Kunwar et
477 al., 2019). However, increased emissions of precursor species during different times of the year
478 may affect these trends (Hyder et al., 2012). Sets MO7, MO8, MO11, and MO14 had the highest
479 contribution to the water-soluble organics from phthalate (range: 9.5 – 10.2%). In contrast, the
480 remaining sets had a much lower contribution (range: 1.7 – 4.9%). However, the absolute
481 concentration of phthalate was highest in sets MO7, MO8, and MO14 (range: 45.3 – 67.0 ng m⁻³)
482 and much lower for the remaining sets (range: 2.0 – 8.9 ng m⁻³). Increased phthalate
483 concentrations during biomass burning episodes have been previously measured in SE Asia (Cao
484 et al., 2017). Furthermore, cloud coverage was fairly low during MO14 as compared to the other
485 sets of interest (Figure 1), increasing the possibility of photochemical production of phthalate.
486 For the remaining sample sets, the range of phthalate concentrations is substantially lower and
487 fairly consistent, indicating that the measured phthalate in these samples most likely represents
488 the local background conditions.

489 While not a carboxylic acid, MSA is nonetheless an important organic aerosol species,
490 especially in marine environments. The assumed precursor of MSA in this study is from the
491 oxidation of marine-emitted dimethylsulfide (DMS). Interestingly, all sample sets showed
492 approximately the same mass percent contribution of MSA to the organic aerosol, ranging from a
493 minimum of 3.1% (MO6) to a maximum of 7.0% (MO5). However, the absolute concentration
494 of MSA was highest in the two sets with biomass burning influence (MO7: 23.3 ng m⁻³ and
495 MO8: 21.4 ng m⁻³), with concentrations 8.4 and 7.7 times higher, respectively, than the lowest
496 MSA concentration measured (MO11: 2.8 ng m⁻³). A previous study showed that MSA
497 concentrations in air masses with mixed influence from marine and biomass burning emissions
498 are higher than the concentrations measured from either source alone (Sorooshian et al., 2015).
499 The results from the present study (i.e. more MSA measured in sets with biomass burning
500 influence) in SE Asia again highlight the complexity of interactions between air masses with
501 different sources and the accompanying changes in aerosol physicochemical properties.

502 503 **4. Conclusions**

504 This study sought to characterize influences of local and long-range transported aerosol
505 to the Philippines during the Southwest Monsoon (SWM) season as well as the various synoptic
506 and local scale conditions that facilitate and suppress long-range transport of aerosol. As a highly



507 populated mega-city, Metro Manila is the source of a large amount of urban, anthropogenic
508 pollution. However, synoptic-scale weather, including the typical SWM flow and typhoons, can
509 impact the transport of aerosol to and from Metro Manila. While previous work in a rural area in
510 the northwest edge of the Philippines has identified seasonal aerosol transport patterns to the
511 Philippines using PM_{2.5} data (Bagtasa et al., 2018), the present study highlights case studies of in
512 situ size-resolved aerosol measurements from Metro Manila to examine the potential for aerosol
513 transport to impact this urban area as well.

514 For two of the sample sets with enhanced total water-soluble aerosol mass concentration,
515 biomass burning aerosol transport from the Maritime Continent (MC) towards the Philippines
516 was identified using air mass back-trajectories and the Navy Aerosol Analysis and Prediction
517 System (NAAPS) model. This transport followed a southwesterly flow pattern that is typical of
518 this time of year (Figure S1) and lends its name to the SWM season. Deep aerosol layers,
519 extending from the surface to 3 km, were identified by CALIOP to the southwest of the
520 Philippines. The influence on aerosol in Metro Manila was shown through enhancements in
521 biomass burning tracer species (e.g. K, Rb) and increased concentration of organic aerosol. The
522 challenges in satellite-based retrievals of biomass burning in the region (Reid et al., 2012, 2013)
523 and the underestimation of fire activity in the region by these satellite retrievals (Reid et al.,
524 2013) lead to unanswered questions about the amount and fate of biomass burning emissions in
525 the MC and SE Asia. The ability to measure biomass burning signatures in a highly polluted,
526 urban mega-city such as Metro Manila and the evidence of long-range transport gathered through
527 multiple methods and data sources (i.e. in situ measurements, models, and remote-sensing)
528 speaks to the strong signature of biomass burning emissions in the region and the long-range
529 transport pathways available for these emissions.

530 In contrast, transport of anthropogenic emissions from continental East Asia was
531 identified on two occasions with high water-soluble aerosol mass concentrations, with one
532 measured instance of long-range transport having been facilitated by the influence of a typhoon.
533 In these cases, it is difficult to separate urban emissions between local and distant sources.
534 However, the elevation of select tracer species (Ba, V, Pb, Mo, Sn) and the water-soluble organic
535 aerosol characteristics for these two cases (i.e. high relative contribution of oxalate to the organic
536 aerosol) indicated that long-range transported urban emissions could impact Metro Manila.

537 Finally, one low aerosol loading case was impacted by air masses travelling over the
538 open ocean to the east of the Philippines. This case showed an enhanced fraction of
539 supermicrometer aerosol and a very low concentration of water-soluble organic acids. Higher
540 rain accumulation during this sample set, as opposed to the sample sets with the highest water-
541 soluble aerosol concentrations, could have led to greater wet scavenging of aerosol. This case
542 also had the lowest overall mass concentration of water-soluble organic species, a low percent
543 contribution of oxalate to the water-soluble organics, and a high percent contribution of maleate.
544 This result points to the relative importance of locally-emitted species that have not yet
545 undergone photochemical and aqueous processing mechanisms that lead to the degradation of
546 longer-chain dicarboxylic acid species into oxalate.

547 These results have important implications for better understanding the aerosol budget and
548 influences in and around the Philippines and SE Asia. Transport of aerosol both into and out of
549 Metro Manila can impact human health, cloud condensation nuclei (CCN) budgets, and radiative
550 forcing in the region. Furthermore, the identification of various tracer species (e.g. K and Rb for
551 biomass burning) and the impacts of different long-range transport mechanisms, and associated
552 mixing of different air mass types, on the water-soluble aerosol characteristics (e.g. enhanced



553 oxalate in emissions from continental regions, enhanced MSA during periods of biomass burning
554 influence) have worldwide applications. As remote-sensing measurements in this region are
555 notoriously difficult (e.g. Reid et al., 2009, 2013), in situ and model results lend vital data to
556 address the questions surrounding characteristics of aerosol that are transported into and out of
557 this highly-populated region.

558

559 *Data availability:* All data used in this work are available upon request.

560

561 *Author Contribution:* MTC, MOC, JBS, RAB, ABM, CS, and AS designed the experiments and
562 all co-authors carried out some aspect of the data collection. MTC, RAB, CS, and AS conducted
563 data analysis and interpretation. RAB and AS prepared the manuscript with contributions from
564 all co-authors.

565

566 *Competing interests:* The authors declare that they have no conflict of interest.

567

568 *Acknowledgements:* This research was funded by NASA grant 80NSSC18K0148. R. A. Braun
569 acknowledges support from the ARCS Foundation. M. T. Cruz acknowledges support from the
570 Philippine Department of Science and Technology's ASTHRD Program. A. B. MacDonald
571 acknowledges support from the Mexican National Council for Science and Technology
572 (CONACYT). We acknowledge Agilent Technologies for their support and Shane Snyder's
573 laboratories for ICP-QQQ data.

574

575 **References**

576

577 Aggarwal, S. G., and Kawamura, K.: Molecular distributions and stable carbon isotopic
578 compositions of dicarboxylic acids and related compounds in aerosols from Sapporo, Japan:
579 Implications for photochemical aging during long-range atmospheric transport, *J. Geophys. Res.-*
580 *Atmos.*, 113, 10.1029/2007jd009365, 2008.

581

582 Agrawal, H., Malloy, Q. G. J., Welch, W. A., Wayne Miller, J., and Cocker, D. R.: In-use
583 gaseous and particulate matter emissions from a modern ocean going container vessel, *Atmos.*
584 *Environ.*, 42, 5504-5510, <https://doi.org/10.1016/j.atmosenv.2008.02.053>, 2008.

585

586 Akagi, S. K., Craven, J. S., Taylor, J. W., McMeeking, G. R., Yokelson, R. J., Burling, I. R.,
587 Urbanski, S. P., Wold, C. E., Seinfeld, J. H., Coe, H., Alvarado, M. J., and Weise, D. R.:
588 Evolution of trace gases and particles emitted by a chaparral fire in California, *Atmos. Chem.*
589 *Phys.*, 12, 1397-1421, 10.5194/acp-12-1397-2012, 2012.

590

591 Alas, H. D., Müller, T., Birmili, W., Kecorius, S., Cambaliza, M. O., Simpas, J. B. B., Cayetano,
592 M., Weinhold, K., Vallar, E., Galvez, M. C., and Wiedensohler, A.: Spatial Characterization of
593 Black Carbon Mass Concentration in the Atmosphere of a Southeast Asian Megacity: An Air
594 Quality Case Study for Metro Manila, Philippines, *Aerosol Air Qual. Res.*, 18, 2301-2317,
595 10.4209/aaqr.2017.08.0281, 2018.

596



- 597 Allen, A. G., Nemitz, E., Shi, J. P., Harrison, R. M., and Greenwood, J. C.: Size distributions of
598 trace metals in atmospheric aerosols in the United Kingdom, *Atmos. Environ.*, 35, 4581-4591,
599 [https://doi.org/10.1016/S1352-2310\(01\)00190-X](https://doi.org/10.1016/S1352-2310(01)00190-X), 2001.
600
- 601 Amato, F., Pandolfi, M., Viana, M., Querol, X., Alastuey, A., and Moreno, T.: Spatial and
602 chemical patterns of PM₁₀ in road dust deposited in urban environment, *Atmos. Environ.*, 43,
603 1650-1659, <https://doi.org/10.1016/j.atmosenv.2008.12.009>, 2009.
604
- 605 Andreae, M. O.: Soot Carbon and Excess Fine Potassium: Long-Range Transport of
606 Combustion-Derived Aerosols, *Science*, 220, 1148, [10.1126/science.220.4602.1148](https://doi.org/10.1126/science.220.4602.1148), 1983.
607
- 608 Arimoto, R., Duce, R. A., Ray, B. J., Ellis Jr, W. G., Cullen, J. D., and Merrill, J. T.: Trace
609 elements in the atmosphere over the North Atlantic, *J. Geophys. Res.-Atmos.*, 100, 1199-1213,
610 [10.1029/94jd02618](https://doi.org/10.1029/94jd02618), 1995.
611
- 612 Artaxo, P., Gerab, F., Yamasoe, M. A., and Martins, J. V.: Fine mode aerosol composition at
613 three long-term atmospheric monitoring sites in the Amazon Basin, *J. Geophys. Res.-Atmos.*, 99,
614 22857-22868, [10.1029/94jd01023](https://doi.org/10.1029/94jd01023), 1994.
615
- 616 Artaxo, P., Oyola, P., and Martinez, R.: Aerosol composition and source apportionment in
617 Santiago de Chile, *Nucl. Instrum. Meth. B*, 150, 409-416, [https://doi.org/10.1016/S0168-583X\(98\)01078-7](https://doi.org/10.1016/S0168-583X(98)01078-7), 1999.
618
- 619
- 620 Atwood, S. A., Reid, J. S., Kreidenweis, S. M., Cliff, S. S., Zhao, Y., Lin, N.-H., Tsay, S.-C.,
621 Chu, Y.-C., and Westphal, D. L.: Size resolved measurements of springtime aerosol particles
622 over the northern South China Sea, *Atmos. Environ.*, 78, 134-143,
623 <https://doi.org/10.1016/j.atmosenv.2012.11.024>, 2013.
624
- 625 Atwood, S. A., Reid, J. S., Kreidenweis, S. M., Blake, D. R., Jonsson, H. H., Lagrosas, N. D.,
626 Xian, P., Reid, E. A., Sessions, W. R., and Simpas, J. B.: Size-resolved aerosol and cloud
627 condensation nuclei (CCN) properties in the remote marine South China Sea – Part 1:
628 Observations and source classification, *Atmos. Chem. Phys.*, 17, 1105-1123, [10.5194/acp-17-1105-2017](https://doi.org/10.5194/acp-17-1105-2017), 2017.
629
- 630
- 631 Bagtasa, G., Cayetano, M. G., and Yuan, C. S.: Seasonal variation and chemical characterization
632 of PM_{2.5} in northwestern Philippines, *Atmos. Chem. Phys.*, 18, 4965-4980, [10.5194/acp-18-4965-2018](https://doi.org/10.5194/acp-18-4965-2018), 2018.
633
- 634
- 635 Balla, D., Voutsas, D., and Samara, C.: Study of polar organic compounds in airborne particulate
636 matter of a coastal urban city, *Environ. Sci. Pollut. R.*, 25, 12191-12205, [10.1007/s11356-017-9993-2](https://doi.org/10.1007/s11356-017-9993-2), 2018.
637
- 638
- 639 Bautista, A. T., Pabroa, P. C. B., Santos, F. L., Racho, J. M. D., and Quirit, L. L.: Carbonaceous
640 particulate matter characterization in an urban and a rural site in the Philippines, *Atmos. Pollut.
641 Res.*, 5, 245-252, <https://doi.org/10.5094/APR.2014.030>, 2014.
642



- 643 Bovallius, A., Bucht, B., Roffey, R., and Anäs, P.: Long-range air transmission of bacteria, *Appl.*
644 *Environ. Microb.*, 35, 1231, 1978.
- 645
- 646 Braun, R. A., Dadashazar, H., MacDonald, A. B., Aldhaif, A. M., Maudlin, L. C., Crosbie, E.,
647 Aghdam, M. A., Hossein Mardi, A., and Sorooshian, A.: Impact of Wildfire Emissions on
648 Chloride and Bromide Depletion in Marine Aerosol Particles, *Environ. Sci. Technol.*, 51, 9013-
649 9021, 10.1021/acs.est.7b02039, 2017.
- 650
- 651 Brito, J., Freney, E., Dominutti, P., Borbon, A., Haslett, S. L., Batenburg, A. M., Colomb, A.,
652 Dupuy, R., Denjean, C., Burnet, F., Bourriane, T., Deroubaix, A., Sellegri, K., Borrmann, S.,
653 Coe, H., Flamant, C., Knippertz, P., and Schwarzenboeck, A.: Assessing the role of
654 anthropogenic and biogenic sources on PM1 over southern West Africa using aircraft
655 measurements, *Atmos. Chem. Phys.*, 18, 757-772, 10.5194/acp-18-757-2018, 2018.
- 656
- 657 Campbell, J. R., Reid, J. S., Westphal, D. L., Zhang, J., Tackett, J. L., Chew, B. N., Welton, E. J.,
658 Shimizu, A., Sugimoto, N., Aoki, K., and Winker, D. M.: Characterizing the vertical profile of
659 aerosol particle extinction and linear depolarization over Southeast Asia and the Maritime
660 Continent: The 2007–2009 view from CALIOP, *Atmos. Res.*, 122, 520-543,
661 <https://doi.org/10.1016/j.atmosres.2012.05.007>, 2013.
- 662
- 663 Cao, F., Zhang, S.-C., Kawamura, K., Liu, X., Yang, C., Xu, Z., Fan, M., Zhang, W., Bao, M.,
664 Chang, Y., Song, W., Liu, S., Lee, X., Li, J., Zhang, G., and Zhang, Y.-L.: Chemical
665 characteristics of dicarboxylic acids and related organic compounds in PM2.5 during biomass-
666 burning and non-biomass-burning seasons at a rural site of Northeast China, *Environ. Pollut.*,
667 231, 654-662, <https://doi.org/10.1016/j.envpol.2017.08.045>, 2017.
- 668
- 669 Cayan, E. O., Chen, T.-C., Argete, J. C., Yen, M.-C., and Nilo, P. D.: The Effect of Tropical
670 Cyclones on Southwest Monsoon Rainfall in the Philippines, *J. Meteorol. Soc. Jpn. Ser. II*, 89A,
671 123-139, 10.2151/jmsj.2011-A08, 2011.
- 672
- 673 Chang, L. T.-C., Tsai, J.-H., Lin, J.-M., Huang, Y.-S., and Chiang, H.-L.: Particulate matter and
674 gaseous pollutants during a tropical storm and air pollution episode in Southern Taiwan, *Atmos.*
675 *Res.*, 99, 67-79, <https://doi.org/10.1016/j.atmosres.2010.09.002>, 2011.
- 676
- 677 Cheng, C., Li, M., Chan, C. K., Tong, H., Chen, C., Chen, D., Wu, D., Li, L., Wu, C., Cheng, P.,
678 Gao, W., Huang, Z., Li, X., Zhang, Z., Fu, Z., Bi, Y., and Zhou, Z.: Mixing state of oxalic acid
679 containing particles in the rural area of Pearl River Delta, China: implications for the formation
680 mechanism of oxalic acid, *Atmos. Chem. Phys.*, 17, 9519-9533, 10.5194/acp-17-9519-2017,
681 2017.
- 682
- 683 Chow, J. C., Watson, J. G., Kuhns, H., Etyemezian, V., Lowenthal, D. H., Crow, D., Kohl, S. D.,
684 Engelbrecht, J. P., and Green, M. C.: Source profiles for industrial, mobile, and area sources in
685 the Big Bend Regional Aerosol Visibility and Observational study, *Chemosphere*, 54, 185-208,
686 <https://doi.org/10.1016/j.chemosphere.2003.07.004>, 2004.
- 687



- 688 Chuang, M.-T., Chang, S.-C., Lin, N.-H., Wang, J.-L., Sheu, G.-R., Chang, Y.-J., and Lee, C.-T.:
689 Aerosol chemical properties and related pollutants measured in Dongsha Island in the northern
690 South China Sea during 7-SEAS/Dongsha Experiment, *Atmos. Environ.*, 78, 82-92,
691 <https://doi.org/10.1016/j.atmosenv.2012.05.014>, 2013.
692
- 693 Crahan, K. K., Hegg, D., Covert, D. S., and Jonsson, H.: An exploration of aqueous oxalic acid
694 production in the coastal marine atmosphere, *Atmos. Environ.*, 38, 3757-3764,
695 <https://doi.org/10.1016/j.atmosenv.2004.04.009>, 2004.
696
- 697 Cruz, F. T., Narisma, G. T., Villafuerte, M. Q., Cheng Chua, K. U., and Olaguera, L. M.: A
698 climatological analysis of the southwest monsoon rainfall in the Philippines, *Atmos. Res.*, 122,
699 609-616, <https://doi.org/10.1016/j.atmosres.2012.06.010>, 2013.
700
- 701 Cruz, M. T., Bañaga, P. A., Betito, G., Braun, R. A., Stahl, C., Aghdam, M. A., Cambaliza, M.
702 O., Dadashazar, H., Hilario, M. R., Lorenzo, G. R., Ma, L., MacDonald, A. B., Pabroa, P. C.,
703 Yee, J. R., Simpas, J. B., and Sorooshian, A.: Size-resolved Composition and Morphology of
704 Particulate Matter During the Southwest Monsoon in Metro Manila, Philippines, *Atmos. Chem.*
705 *Phys.*, 19, 10675-10696, <https://doi.org/10.5194/acp-19-10675-2019>, 2019.
706
- 707 Dave, P., Bhushan, M., and Venkataraman, C.: Aerosols cause intraseasonal short-term
708 suppression of Indian monsoon rainfall, *Sci. Rep.-UK*, 7, 17347, [10.1038/s41598-017-17599-1](https://doi.org/10.1038/s41598-017-17599-1),
709 2017.
710
- 711 Deshmukh, D. K., Deb, M. K., Hopke, P. K., and Tsai, Y. I.: Seasonal Characteristics of Water-
712 Soluble Dicarboxylates Associated with PM₁₀ in the Urban Atmosphere of Durg City, India,
713 *Aerosol Air Qual. Res.*, 12, 683-696, [10.4209/aaqr.2012.02.0040](https://doi.org/10.4209/aaqr.2012.02.0040), 2012.
714
- 715 Deshmukh, D. K., Mozammel Haque, M., Kawamura, K., and Kim, Y.: Dicarboxylic acids,
716 oxocarboxylic acids and α -dicarbonyls in fine aerosols over central Alaska: Implications for
717 sources and atmospheric processes, *Atmos. Res.*, 202, 128-139,
718 <https://doi.org/10.1016/j.atmosres.2017.11.003>, 2018.
719
- 720 Duce, R. A., Liss, P. S., Merrill, J. T., Atlas, E. L., Buat-Menard, P., Hicks, B. B., Miller, J. M.,
721 Prospero, J. M., Arimoto, R., Church, T. M., Ellis, W., Galloway, J. N., Hansen, L., Jickells, T.
722 D., Knap, A. H., Reinhardt, K. H., Schneider, B., Soudine, A., Tokos, J. J., Tsunogai, S.,
723 Wollast, R., and Zhou, M.: The atmospheric input of trace species to the world ocean, *Global*
724 *Biogeochem. Cy.*, 5, 193-259, [10.1029/91gb01778](https://doi.org/10.1029/91gb01778), 1991.
725
- 726 Echalar, F., Gaudichet, A., Cachier, H., and Artaxo, P.: Aerosol emissions by tropical forest and
727 savanna biomass burning: Characteristic trace elements and fluxes, *Geophys. Res. Lett.*, 22,
728 3039-3042, [10.1029/95gl03170](https://doi.org/10.1029/95gl03170), 1995.
729
- 730 Ervens, B.: Modeling the Processing of Aerosol and Trace Gases in Clouds and Fogs, *Chem.*
731 *Rev.*, 115, 4157-4198, [10.1021/cr5005887](https://doi.org/10.1021/cr5005887), 2015.
732



- 733 Ervens, B., Feingold, G., Frost, G. J., and Kreidenweis, S. M.: A modeling study of aqueous
734 production of dicarboxylic acids: 1. Chemical pathways and speciated organic mass production,
735 *J. Geophys. Res.-Atmos.*, 109, 10.1029/2003jd004387, 2004.
736
- 737 Ervens, B., Sorooshian, A., Aldhaif, A. M., Shingler, T., Crosbie, E., Ziemba, L., Campuzano-
738 Jost, P., Jimenez, J. L., and Wisthaler, A.: Is there an aerosol signature of chemical cloud
739 processing?, *Atmos. Chem. Phys.*, 18, 16099-16119, 10.5194/acp-18-16099-2018, 2018.
740
- 741 Falkovich, A. H., Graber, E. R., Schkolnik, G., Rudich, Y., Maenhaut, W., and Artaxo, P.: Low
742 molecular weight organic acids in aerosol particles from Rondônia, Brazil, during the biomass-
743 burning, transition and wet periods, *Atmos. Chem. Phys.*, 5, 781-797, 10.5194/acp-5-781-2005,
744 2005.
745
- 746 Fang, G.-C., Lin, S.-J., Chang, S.-Y., and Chou, C.-C. K.: Effect of typhoon on atmospheric
747 particulates in autumn in central Taiwan, *Atmos. Environ.*, 43, 6039-6048,
748 <https://doi.org/10.1016/j.atmosenv.2009.08.033>, 2009.
749
- 750 Farren, N. J., Dunmore, R. E., Mead, M. I., Mohd Nadzir, M. S., Samah, A. A., Phang, S. M.,
751 Bandy, B. J., Sturges, W. T., and Hamilton, J. F.: Chemical characterisation of water-soluble
752 ions in atmospheric particulate matter on the east coast of Peninsular Malaysia, *Atmos. Chem.*
753 *Phys.*, 19, 1537-1553, 10.5194/acp-19-1537-2019, 2019.
754
- 755 Flannigan, M. D., Krawchuk, M. A., de Groot, W. J., Wotton, B. M., and Gowman, L. M.:
756 Implications of changing climate for global wildland fire, *Int. J. Wildland Fire*, 18, 483-507,
757 <https://doi.org/10.1071/WF08187>, 2009.
758
- 759 Flannigan, M., Cantin, A. S., de Groot, W. J., Wotton, M., Newbery, A., and Gowman, L. M.:
760 Global wildland fire season severity in the 21st century, *Forest Ecol. Manag.*, 294, 54-61,
761 <https://doi.org/10.1016/j.foreco.2012.10.022>, 2013.
762
- 763 Fujimori, T., Takigami, H., Agusa, T., Eguchi, A., Bekki, K., Yoshida, A., Terazono, A., and
764 Ballesteros, F. C.: Impact of metals in surface matrices from formal and informal electronic-
765 waste recycling around Metro Manila, the Philippines, and intra-Asian comparison, *J. Hazard.*
766 *Mater.*, 221-222, 139-146, <https://doi.org/10.1016/j.jhazmat.2012.04.019>, 2012.
767
- 768 Fung, Y. S., and Wong, L. W. Y.: Apportionment of air pollution sources by receptor models in
769 Hong Kong, *Atmos. Environ.*, 29, 2041-2048, [https://doi.org/10.1016/1352-2310\(94\)00239-H](https://doi.org/10.1016/1352-2310(94)00239-H),
770 1995.
771
- 772 Gadde, B., Bonnet, S., Menke, C., and Garivait, S.: Air pollutant emissions from rice straw open
773 field burning in India, Thailand and the Philippines, *Environ. Pollut.*, 157, 1554-1558,
774 <https://doi.org/10.1016/j.envpol.2009.01.004>, 2009.
775
- 776 Ge, C., Wang, J., Reid, J. S., Posselt, D. J., Xian, P., and Hyer, E.: Mesoscale modeling of smoke
777 transport from equatorial Southeast Asian Maritime Continent to the Philippines: First



- 778 comparison of ensemble analysis with in situ observations, *J. Geophys. Res.-Atmos.*, 122, 5380-
779 5398, doi:10.1002/2016JD026241, 2017.
- 780
- 781 Gelaro, R., McCarty, W., Suárez, M. J., Todling, R., Molod, A., Takacs, L., Randles, C. A.,
782 Darmenov, A., Bosilovich, M. G., Reichle, R., Wargan, K., Coy, L., Cullather, R., Draper, C.,
783 Akella, S., Buchard, V., Conaty, A., Silva, A. M. d., Gu, W., Kim, G.-K., Koster, R., Lucchesi,
784 R., Merkova, D., Nielsen, J. E., Partyka, G., Pawson, S., Putman, W., Rienecker, M., Schubert,
785 S. D., Sienkiewicz, M., and Zhao, B.: The Modern-Era Retrospective Analysis for Research and
786 Applications, Version 2 (MERRA-2), *J. Climate*, 30, 5419-5454, 10.1175/jcli-d-16-0758.1,
787 2017.
- 788
- 789 Global Modeling and Assimilation Office (GMAO): MERRA-2 inst3_3d_asm_Nv: 3d,3-
790 Hourly,Instantaneous,Model-Level,Assimilation,Assimilated Meteorological Fields V5.12.4,
791 Goddard Earth Sciences Data and Information Services Center (GES DISC),
792 10.5067/WWQSQ8IVFW8, 2015a.
- 793
- 794 Global Modeling and Assimilation Office (GMAO): MERRA-2 tavg1_2d_rad_Nx: 2d,1-
795 Hourly,Time-Averaged,Single-Level,Assimilation,Radiation Diagnostics V5.12.4, Goddard
796 Earth Sciences Data and Information Services Center (GES DISC), 10.5067/Q9QMY5PBNV1T,
797 2015b.
- 798
- 799 Goldstein, A. H., Koven, C. D., Heald, C. L., and Fung, I. Y.: Biogenic carbon and
800 anthropogenic pollutants combine to form a cooling haze over the southeastern United States, *P.*
801 *Natl. Acad. Sci. USA*, 106, 8835-8840, 10.1073/pnas.0904128106, 2009.
- 802
- 803 Graf, H. F., Yang, J., and Wagner, T. M.: Aerosol effects on clouds and precipitation during the
804 1997 smoke episode in Indonesia, *Atmos. Chem. Phys.*, 9, 743-756, 10.5194/acp-9-743-2009,
805 2009.
- 806
- 807 Ho, K. F., Lee, S. C., Cao, J. J., Kawamura, K., Watanabe, T., Cheng, Y., and Chow, J. C.:
808 Dicarboxylic acids, ketocarboxylic acids and dicarbonyls in the urban roadside area of Hong
809 Kong, *Atmos. Environ.*, 40, 3030-3040, <https://doi.org/10.1016/j.atmosenv.2005.11.069>, 2006.
- 810
- 811 Hogan, T. F., Liu, M., Ridout, J. A., Peng, M. S., Whitcomb, T. R., Ruston, B. C., Reynolds, C.
812 A., Eckermann, S. D., Moskaitis, J. R., Baker, N. L., McCormack, J. P., Viner, K. C., McLay, J.
813 G., Flatau, M. K., Xu, L., Chen, C., and Chang, S. W.: The Navy Global Environmental Model,
814 *Oceanography*, 27, 116-125, <https://doi.org/10.5670/oceanog.2014.73>, 2014.
- 815
- 816 Hong, Y., Hsu, K.-L., Sorooshian, S., and Gao, X.: Precipitation Estimation from Remotely
817 Sensed Imagery Using an Artificial Neural Network Cloud Classification System, *J. Appl.*
818 *Meteorol.*, 43, 1834-1853, 10.1175/jam2173.1, 2004.
- 819
- 820 Hoque, M. M. M., Kawamura, K., and Uematsu, M.: Spatio-temporal distributions of
821 dicarboxylic acids, ω -oxocarboxylic acids, pyruvic acid, α -dicarbonyls and fatty acids in the
822 marine aerosols from the North and South Pacific, *Atmos. Res.*, 185, 158-168,
823 <https://doi.org/10.1016/j.atmosres.2016.10.022>, 2017.



- 824
825 Hsieh, L.-Y., Kuo, S.-C., Chen, C.-L., and Tsai, Y. I.: Origin of low-molecular-weight
826 dicarboxylic acids and their concentration and size distribution variation in suburban aerosol,
827 *Atmos. Environ.*, 41, 6648-6661, <https://doi.org/10.1016/j.atmosenv.2007.04.014>, 2007.
828
829 Hsieh, L.-Y., Chen, C.-L., Wan, M.-W., Tsai, C.-H., and Tsai, Y. I.: Speciation and temporal
830 characterization of dicarboxylic acids in PM_{2.5} during a PM episode and a period of non-
831 episodic pollution, *Atmos. Environ.*, 42, 6836-6850,
832 <https://doi.org/10.1016/j.atmosenv.2008.05.021>, 2008.
833
834 Hyder, M., Genberg, J., Sandahl, M., Swietlicki, E., and Jönsson, J. Å.: Yearly trend of
835 dicarboxylic acids in organic aerosols from south of Sweden and source attribution, *Atmos.*
836 *Environ.*, 57, 197-204, <https://doi.org/10.1016/j.atmosenv.2012.04.027>, 2012.
837
838 Jeong, C.-H., Wang, J. M., Hilker, N., Deboisz, J., Sofowote, U., Su, Y., Noble, M., Healy, R. M.,
839 Munoz, T., Dabek-Zlotorzynska, E., Celo, V., White, L., Audette, C., Herod, D., and Evans, G.
840 J.: Temporal and spatial variability of traffic-related PM_{2.5} sources: Comparison of exhaust and
841 non-exhaust emissions, *Atmos. Environ.*, 198, 55-69,
842 <https://doi.org/10.1016/j.atmosenv.2018.10.038>, 2019.
843
844 Juneng, L., Latif, M. T., and Tangang, F.: Factors influencing the variations of PM₁₀ aerosol
845 dust in Klang Valley, Malaysia during the summer, *Atmos. Environ.*, 45, 4370-4378,
846 <https://doi.org/10.1016/j.atmosenv.2011.05.045>, 2011.
847
848 Kawamura, K., and Ikushima, K.: Seasonal changes in the distribution of dicarboxylic acids in
849 the urban atmosphere, *Environ. Sci. Technol.*, 27, 2227-2235, [10.1021/es00047a033](https://doi.org/10.1021/es00047a033), 1993.
850
851 Kawamura, K., and Kaplan, I. R.: Motor exhaust emissions as a primary source for dicarboxylic
852 acids in Los Angeles ambient air, *Environ. Sci. Technol.*, 21, 105-110, [10.1021/es00155a014](https://doi.org/10.1021/es00155a014),
853 1987.
854
855 Kawamura, K., and Sakaguchi, F.: Molecular distributions of water soluble dicarboxylic acids in
856 marine aerosols over the Pacific Ocean including tropics, *J. Geophys. Res.-Atmos.*, 104, 3501-
857 3509, [10.1029/1998jd100041](https://doi.org/10.1029/1998jd100041), 1999.
858
859 Kawamura, K., Kasukabe, H., and Barrie, L. A.: Source and reaction pathways of dicarboxylic
860 acids, ketoacids and dicarbonyls in arctic aerosols: One year of observations, *Atmos. Environ.*,
861 30, 1709-1722, [https://doi.org/10.1016/1352-2310\(95\)00395-9](https://doi.org/10.1016/1352-2310(95)00395-9), 1996.
862
863 Kecorius, S., Madueño, L., Vallar, E., Alas, H., Betito, G., Birmili, W., Cambaliza, M. O.,
864 Catipay, G., Gonzaga-Cayetano, M., Galvez, M. C., Lorenzo, G., Müller, T., Simpas, J. B.,
865 Tamayo, E. G., and Wiedensohler, A.: Aerosol particle mixing state, refractory particle number
866 size distributions and emission factors in a polluted urban environment: Case study of Metro
867 Manila, Philippines, *Atmos. Environ.*, 170, 169-183,
868 <https://doi.org/10.1016/j.atmosenv.2017.09.037>, 2017.
869



- 870 Kim, E., and Hopke, P. K.: Source characterization of ambient fine particles at multiple sites in
871 the Seattle area, *Atmos. Environ.*, 42, 6047-6056,
872 <https://doi.org/10.1016/j.atmosenv.2008.03.032>, 2008.
873
- 874 Kim, J. Y., Ghim, Y. S., Song, C. H., Yoon, S.-C., and Han, J. S.: Seasonal characteristics of air
875 masses arriving at Gosan, Korea, using fine particle measurements between November 2001 and
876 August 2003, *J. Geophys. Res.-Atmos.*, 112, 10.1029/2005jd006946, 2007.
877
- 878 Kim Oanh, N. T., Upadhyay, N., Zhuang, Y. H., Hao, Z. P., Murthy, D. V. S., Lestari, P.,
879 Villarín, J. T., Chengchua, K., Co, H. X., Dung, N. T., and Lindgren, E. S.: Particulate air
880 pollution in six Asian cities: Spatial and temporal distributions, and associated sources, *Atmos.*
881 *Environ.*, 40, 3367-3380, <https://doi.org/10.1016/j.atmosenv.2006.01.050>, 2006.
882
- 883 Kristiansen, N. I., Stohl, A., Olivié, D. J. L., Croft, B., Søvde, O. A., Klein, H., Christoudias, T.,
884 Kunkel, D., Leadbetter, S. J., Lee, Y. H., Zhang, K., Tsigaridis, K., Bergman, T., Evangelioú, N.,
885 Wang, H., Ma, P. L., Easter, R. C., Rasch, P. J., Liu, X., Pitari, G., Di Genova, G., Zhao, S. Y.,
886 Balkanski, Y., Bauer, S. E., Faluvegi, G. S., Kokkola, H., Martin, R. V., Pierce, J. R., Schulz, M.,
887 Shindell, D., Tost, H., and Zhang, H.: Evaluation of observed and modelled aerosol lifetimes
888 using radioactive tracers of opportunity and an ensemble of 19 global models, *Atmos. Chem.*
889 *Phys.*, 16, 3525-3561, 10.5194/acp-16-3525-2016, 2016.
890
- 891 Kumar, S., Aggarwal, S. G., Gupta, P. K., and Kawamura, K.: Investigation of the tracers for
892 plastic-enriched waste burning aerosols, *Atmos. Environ.*, 108, 49-58,
893 <https://doi.org/10.1016/j.atmosenv.2015.02.066>, 2015.
894
- 895 Kunwar, B., Kawamura, K., Fujiwara, S., Fu, P., Miyazaki, Y., and Pokhrel, A.: Dicarboxylic
896 acids, oxocarboxylic acids and α -dicarbonyls in atmospheric aerosols from Mt. Fuji, Japan:
897 Implication for primary emission versus secondary formation, *Atmos. Res.*, 221, 58-71,
898 <https://doi.org/10.1016/j.atmosres.2019.01.021>, 2019.
899
- 900 Latif, M. T., Othman, M., Idris, N., Juneng, L., Abdullah, A. M., Hamzah, W. P., Khan, M. F.,
901 Nik Sulaiman, N. M., Jewaratnam, J., Aghamohammadi, N., Sahani, M., Xiang, C. J., Ahamad,
902 F., Amil, N., Darus, M., Varkkey, H., Tangang, F., and Jaafar, A. B.: Impact of regional haze
903 towards air quality in Malaysia: A review, *Atmos. Environ.*, 177, 28-44,
904 <https://doi.org/10.1016/j.atmosenv.2018.01.002>, 2018.
905
- 906 Li, X.-d., Yang, Z., Fu, P., Yu, J., Lang, Y.-c., Liu, D., Ono, K., and Kawamura, K.: High
907 abundances of dicarboxylic acids, oxocarboxylic acids, and α -dicarbonyls in fine aerosols
908 (PM_{2.5}) in Chengdu, China during wintertime haze pollution, *Environ. Sci. Pollut. R.*, 22,
909 12902-12918, 10.1007/s11356-015-4548-x, 2015.
910
- 911 Lin, C.-C., Chen, S.-J., Huang, K.-L., Hwang, W.-I., Chang-Chien, G.-P., and Lin, W.-Y.:
912 Characteristics of Metals in Nano/Ultrafine/Fine/Coarse Particles Collected Beside a Heavily
913 Trafficked Road, *Environ. Sci. Technol.*, 39, 8113-8122, 10.1021/es048182a, 2005.
914



- 915 Lin, C. Y., Hsu, H. m., Lee, Y. H., Kuo, C. H., Sheng, Y. F., and Chu, D. A.: A new transport
916 mechanism of biomass burning from Indochina as identified by modeling studies, *Atmos. Chem.*
917 *Phys.*, 9, 7901-7911, 10.5194/acp-9-7901-2009, 2009.
918
- 919 Lin, I. I., Chen, J.-P., Wong, G. T. F., Huang, C.-W., and Lien, C.-C.: Aerosol input to the South
920 China Sea: Results from the MODerate Resolution Imaging Spectro-radiometer, the Quick
921 Scatterometer, and the Measurements of Pollution in the Troposphere Sensor, *Deep-Sea Res. Pt.*
922 *II*, 54, 1589-1601, <https://doi.org/10.1016/j.dsr2.2007.05.013>, 2007.
923
- 924 Lindqvist, O., Johansson, K., Bringmark, L., Timm, B., Aastrup, M., Andersson, A., Hovsenius,
925 G., Håkanson, L., Iverfeldt, Å., and Meili, M.: Mercury in the Swedish environment — Recent
926 research on causes, consequences and corrective methods, *Water Air Soil Poll.*, 55, xi-261,
927 10.1007/bf00542429, 1991.
928
- 929 Liu, W., Han, Y., Yin, Y., Duan, J., Gong, J., Liu, Z., and Xu, W.: An aerosol air pollution
930 episode affected by binary typhoons in east and central China, *Atmos. Pollut. Res.*, 9, 634-642,
931 <https://doi.org/10.1016/j.apr.2018.01.005>, 2018.
932
- 933 Liu, Y., Cai, W., Sun, C., Song, H., Cobb, K. M., Li, J., Leavitt, S. W., Wu, L., Cai, Q., Liu, R.,
934 Ng, B., Cherubini, P., Büentgen, U., Song, Y., Wang, G., Lei, Y., Yan, L., Li, Q., Ma, Y., Fang,
935 C., Sun, J., Li, X., Chen, D., and Linderholm, H. W.: Anthropogenic aerosols cause recent
936 pronounced weakening of Asian Summer Monsoon relative to last four centuries, *Geophys. Res.*
937 *Lett.*, 46, 10.1029/2019gl082497, 2019.
938
- 939 Lu, C.-C., Yuan, C.-S., and Li, T.-C.: How Aeolian Dust Deteriorate Ambient Particulate Air
940 Quality along an Expansive River Valley in Southern Taiwan? A Case Study of Typhoon
941 Doksuri, *Aerosol Air Qual. Res.*, 17, 2181-2196, 10.4209/aaqr.2017.08.0257, 2017.
942
- 943 Lynch, P., Reid, J. S., Westphal, D. L., Zhang, J., Hogan, T. F., Hyer, E. J., Curtis, C. A., Hegg,
944 D. A., Shi, Y., Campbell, J. R., Rubin, J. I., Sessions, W. R., Turk, F. J., and Walker, A. L.: An
945 11-year global gridded aerosol optical thickness reanalysis (v1.0) for atmospheric and climate
946 sciences, *Geosci. Model Dev.*, 9, 1489-1522, 10.5194/gmd-9-1489-2016, 2016.
947
- 948 Lyons, W. A., Dooley, J. C., and Whitby, K. T.: Satellite detection of long-range pollution
949 transport and sulfate aerosol hazes, *Atmos. Environ.* (1967), 12, 621-631,
950 [https://doi.org/10.1016/0004-6981\(78\)90242-1](https://doi.org/10.1016/0004-6981(78)90242-1), 1978.
951
- 952 Ma, L., Dadashazar, H., Braun, R. A., MacDonald, A. B., Aghdam, M. A., Maudlin, L. C., and
953 Sorooshian, A.: Size-resolved Characteristics of Water-Soluble Particulate Elements in a Coastal
954 Area: Source Identification, Influence of Wildfires, and Diurnal Variability, *Atmos. Environ.*,
955 <https://doi.org/10.1016/j.atmosenv.2019.02.045>, 2019.
956
- 957 Maenhaut, W., Salma, I., Cafmeyer, J., Annegarn, H. J., and Andreae, M. O.: Regional
958 atmospheric aerosol composition and sources in the eastern Transvaal, South Africa, and impact
959 of biomass burning, *J. Geophys. Res.-Atmos.*, 101, 23631-23650, 10.1029/95jd02930, 1996.
960



- 961 Maki, T., Lee, K. C., Kawai, K., Onishi, K., Hong, C. S., Kurosaki, Y., Shinoda, M., Kai, K.,
962 Iwasaka, Y., Archer, S. D. J., Lacap-Bugler, D. C., Hasegawa, H., and Pointing, S. B.: Aeolian
963 dispersal of bacteria associated with desert dust and anthropogenic particles over continental and
964 oceanic surfaces, *J. Geophys. Res.-Atmos.*, 124, 10.1029/2018jd029597, 2019.
- 965
966 Mamoudou, I., Zhang, F., Chen, Q., Wang, P., and Chen, Y.: Characteristics of PM_{2.5} from ship
967 emissions and their impacts on the ambient air: A case study in Yangshan Harbor, Shanghai, *Sci.*
968 *Total Environ.*, 640-641, 207-216, <https://doi.org/10.1016/j.scitotenv.2018.05.261>, 2018.
- 969
970 Marple, V., Olson, B., Romay, F., Hudak, G., Geerts, S. M., and Lundgren, D.: Second
971 Generation Micro-Orifice Uniform Deposit Impactor, 120 MOUDI-II: Design, Evaluation, and
972 Application to Long-Term Ambient Sampling, *Aerosol Sci. Tech.*, 48, 427-433,
973 10.1080/02786826.2014.884274, 2014.
- 974
975 Maudlin, L. C., Wang, Z., Jonsson, H. H., and Sorooshian, A.: Impact of wildfires on size-
976 resolved aerosol composition at a coastal California site, *Atmos. Environ.*, 119, 59-68,
977 <https://doi.org/10.1016/j.atmosenv.2015.08.039>, 2015.
- 978
979 Mosher, B. W., and Duce, R. A.: A global atmospheric selenium budget, *J. Geophys. Res.-*
980 *Atmos.*, 92, 13289-13298, doi:10.1029/JD092iD11p13289, 1987.
- 981
982 Nguyen, P., Sellars, S., Thorstensen, A., Tao, Y., Ashouri, H., Braithwaite, D., Hsu, K., and
983 Sorooshian, S.: Satellites Track Precipitation of Super Typhoon Haiyan, *Eos Trans. AGU*, 95,
984 133-135, 10.1002/2014eo160002, 2014.
- 985
986 Nguyen, P., Shearer, E. J., Tran, H., Ombadi, M., Hayatbini, N., Palacios, T., Huynh, P.,
987 Braithwaite, D., Updegraff, G., Hsu, K., Kuligowski, B., Logan, W. S., and Sorooshian, S.: The
988 CHRS Data Portal, an easily accessible public repository for PERSIANN global satellite
989 precipitation data, *Scientific Data*, 6, 180296, 10.1038/sdata.2018.296, 2019.
- 990
991 Nirmalkar, J., Deshmukh, D. K., Deb, M. K., Tsai, Y. I., and Sopajaree, K.: Mass loading and
992 episodic variation of molecular markers in PM_{2.5} aerosols over a rural area in eastern central
993 India, *Atmos. Environ.*, 117, 41-50, <https://doi.org/10.1016/j.atmosenv.2015.07.003>, 2015.
- 994
995 Nordø, J.: Long range transport of air pollutants in Europe and acid precipitation in Norway,
996 *Water Air Soil Poll.*, 6, 199-217, 10.1007/bf00182865, 1976.
- 997
998 Pakkanen, T. A., Loukkola, K., Korhonen, C. H., Aurela, M., Mäkelä, T., Hillamo, R. E., Aarnio,
999 P., Koskentalo, T., Kousa, A., and Maenhaut, W.: Sources and chemical composition of
1000 atmospheric fine and coarse particles in the Helsinki area, *Atmos. Environ.*, 35, 5381-5391,
1001 [https://doi.org/10.1016/S1352-2310\(01\)00307-7](https://doi.org/10.1016/S1352-2310(01)00307-7), 2001.
- 1002
1003 Pakkanen, T. A., Kerminen, V.-M., Loukkola, K., Hillamo, R. E., Aarnio, P., Koskentalo, T., and
1004 Maenhaut, W.: Size distributions of mass and chemical components in street-level and rooftop
1005 PM₁ particles in Helsinki, *Atmos. Environ.*, 37, 1673-1690, [https://doi.org/10.1016/S1352-2310\(03\)00011-6](https://doi.org/10.1016/S1352-2310(03)00011-6), 2003.
- 1006



- 1007
1008 Pandolfi, M., Gonzalez-Castanedo, Y., Alastuey, A., de la Rosa, J. D., Mantilla, E., de la Campa,
1009 A. S., Querol, X., Pey, J., Amato, F., and Moreno, T.: Source apportionment of PM₁₀ and PM_{2.5}
1010 at multiple sites in the strait of Gibraltar by PMF: impact of shipping emissions, *Environ. Sci.*
1011 *Pollut. R.*, 18, 260-269, 10.1007/s11356-010-0373-4, 2011.
1012
1013 Querol, X., Alastuey, A., Moreno, T., Viana, M. M., Castillo, S., Pey, J., Rodríguez, S.,
1014 Artiñano, B., Salvador, P., Sánchez, M., Garcia Dos Santos, S., Herce Garraleta, M. D.,
1015 Fernandez-Patier, R., Moreno-Grau, S., Negral, L., Minguillón, M. C., Monfort, E., Sanz, M. J.,
1016 Palomo-Marín, R., Pinilla-Gil, E., Cuevas, E., de la Rosa, J., and Sánchez de la Campa, A.:
1017 Spatial and temporal variations in airborne particulate matter (PM₁₀ and PM_{2.5}) across Spain
1018 1999–2005, *Atmos. Environ.*, 42, 3964-3979, <https://doi.org/10.1016/j.atmosenv.2006.10.071>,
1019 2008.
1020
1021 Ray, J., and McDow, S. R.: Dicarboxylic acid concentration trends and sampling artifacts,
1022 *Atmos. Environ.*, 39, 7906-7919, <https://doi.org/10.1016/j.atmosenv.2005.09.024>, 2005.
1023
1024 Reid, J. S., Hyer, E. J., Prins, E. M., Westphal, D. L., Zhang, J., Wang, J., Christopher, S. A.,
1025 Curtis, C. A., Schmidt, C. C., Eleuterio, D. P., Richardson, K. A., and Hoffman, J. P.: Global
1026 Monitoring and Forecasting of Biomass-Burning Smoke: Description of and Lessons From the
1027 Fire Locating and Modeling of Burning Emissions (FLAMBE) Program, *IEEE J. Sel. Top.*
1028 *Appl.*, 2, 144-162, 10.1109/jstars.2009.2027443, 2009.
1029
1030 Reid, J. S., Xian, P., Hyer, E. J., Flatau, M. K., Ramirez, E. M., Turk, F. J., Sampson, C. R.,
1031 Zhang, C., Fukada, E. M., and Maloney, E. D.: Multi-scale meteorological conceptual analysis of
1032 observed active fire hotspot activity and smoke optical depth in the Maritime Continent, *Atmos.*
1033 *Chem. Phys.*, 12, 2117-2147, 10.5194/acp-12-2117-2012, 2012.
1034
1035 Reid, J. S., Hyer, E. J., Johnson, R. S., Holben, B. N., Yokelson, R. J., Zhang, J., Campbell, J. R.,
1036 Christopher, S. A., Di Girolamo, L., Giglio, L., Holz, R. E., Kearney, C., Miettinen, J., Reid, E.
1037 A., Turk, F. J., Wang, J., Xian, P., Zhao, G., Balasubramanian, R., Chew, B. N., Janjai, S.,
1038 Lagrosas, N., Lestari, P., Lin, N.-H., Mahmud, M., Nguyen, A. X., Norris, B., Oanh, N. T. K.,
1039 Oo, M., Salinas, S. V., Welton, E. J., and Liew, S. C.: Observing and understanding the
1040 Southeast Asian aerosol system by remote sensing: An initial review and analysis for the Seven
1041 Southeast Asian Studies (7SEAS) program, *Atmos. Res.*, 122, 403-468,
1042 <https://doi.org/10.1016/j.atmosres.2012.06.005>, 2013.
1043
1044 Reid, J. S., Lagrosas, N. D., Jonsson, H. H., Reid, E. A., Sessions, W. R., Simpas, J. B., Uy, S.
1045 N., Boyd, T. J., Atwood, S. A., Blake, D. R., Campbell, J. R., Cliff, S. S., Holben, B. N., Holz,
1046 R. E., Hyer, E. J., Lynch, P., Meinardi, S., Posselt, D. J., Richardson, K. A., Salinas, S. V.,
1047 Smirnov, A., Wang, Q., Yu, L., and Zhang, J.: Observations of the temporal variability in aerosol
1048 properties and their relationships to meteorology in the summer monsoonal South China Sea/East
1049 Sea: the scale-dependent role of monsoonal flows, the Madden–Julian Oscillation, tropical
1050 cyclones, squall lines and cold pools, *Atmos. Chem. Phys.*, 15, 1745-1768, 10.5194/acp-15-
1051 1745-2015, 2015.
1052



- 1053 Reid, J. S., Xian, P., Holben, B. N., Hyer, E. J., Reid, E. A., Salinas, S. V., Zhang, J., Campbell,
1054 J. R., Chew, B. N., Holz, R. E., Kuciauskas, A. P., Lagrosas, N., Posselt, D. J., Sampson, C. R.,
1055 Walker, A. L., Welton, E. J., and Zhang, C.: Aerosol meteorology of the Maritime Continent for
1056 the 2012 7SEAS southwest monsoon intensive study – Part 1: regional-scale phenomena, *Atmos.*
1057 *Chem. Phys.*, 16, 14041-14056, 10.5194/acp-16-14041-2016, 2016a.
1058
- 1059 Reid, J. S., Lagrosas, N. D., Jonsson, H. H., Reid, E. A., Atwood, S. A., Boyd, T. J., Ghate, V.
1060 P., Xian, P., Posselt, D. J., Simpas, J. B., Uy, S. N., Zaiger, K., Blake, D. R., Bucholtz, A.,
1061 Campbell, J. R., Chew, B. N., Cliff, S. S., Holben, B. N., Holz, R. E., Hyer, E. J., Kreidenweis,
1062 S. M., Kuciauskas, A. P., Lolli, S., Oo, M., Perry, K. D., Salinas, S. V., Sessions, W. R.,
1063 Smirnov, A., Walker, A. L., Wang, Q., Yu, L., Zhang, J., and Zhao, Y.: Aerosol meteorology of
1064 Maritime Continent for the 2012 7SEAS southwest monsoon intensive study – Part 2: Philippine
1065 receptor observations of fine-scale aerosol behavior, *Atmos. Chem. Phys.*, 16, 14057-14078,
1066 10.5194/acp-16-14057-2016, 2016b.
1067
- 1068 Ross, A. D., Holz, R. E., Quinn, G., Reid, J. S., Xian, P., Turk, F. J., and Posselt, D. J.: Exploring
1069 the first aerosol indirect effect over Southeast Asia using a 10-year collocated MODIS, CALIOP,
1070 and model dataset, *Atmos. Chem. Phys.*, 18, 12747-12764, 10.5194/acp-18-12747-2018, 2018.
1071
- 1072 Satsumabayashi, H., Kurita, H., Yokouchi, Y., and Ueda, H.: Photochemical formation of
1073 particulate dicarboxylic acids under long-range transport in central Japan, *Atmos. Environ.. Part*
1074 *A. General Topics*, 24, 1443-1450, [https://doi.org/10.1016/0960-1686\(90\)90053-P](https://doi.org/10.1016/0960-1686(90)90053-P), 1990.
1075
- 1076 Schlosser, J. S., Braun, R. A., Bradley, T., Dadashazar, H., MacDonald, A. B., Aldhaif, A. A.,
1077 Aghdam, M. A., Mardi, A. H., Xian, P., and Sorooshian, A.: Analysis of aerosol composition
1078 data for western United States wildfires between 2005 and 2015: Dust emissions, chloride
1079 depletion, and most enhanced aerosol constituents, *J. Geophys. Res.-Atmos.*, 122, 8951-8966,
1080 10.1002/2017jd026547, 2017.
1081
- 1082 Simpas, J., Lorenzo, G., and Cruz, M. T.: Monitoring Particulate Matter Levels and Composition
1083 for Source Apportionment Study in Metro Manila, Philippines, in: *Improving Air Quality in*
1084 *Asian Developing Countries: Compilation of Research Findings*, edited by: Kim Oanh, N. T.,
1085 NARENCA, Vietnam Publishing House of Natural Resources, Environment and Cartography,
1086 Vietnam, 239-261, 2014.
1087
- 1088 Singh, M., Jaques, P. A., and Sioutas, C.: Size distribution and diurnal characteristics of particle-
1089 bound metals in source and receptor sites of the Los Angeles Basin, *Atmos. Environ.*, 36, 1675-
1090 1689, [https://doi.org/10.1016/S1352-2310\(02\)00166-8](https://doi.org/10.1016/S1352-2310(02)00166-8), 2002.
1091
- 1092 Song, J., Zhao, Y., Zhang, Y., Fu, P., Zheng, L., Yuan, Q., Wang, S., Huang, X., Xu, W., Cao,
1093 Z., Gromov, S., and Lai, S.: Influence of biomass burning on atmospheric aerosols over the
1094 western South China Sea: Insights from ions, carbonaceous fractions and stable carbon isotope
1095 ratios, *Environ. Pollut.*, 242, 1800-1809, <https://doi.org/10.1016/j.envpol.2018.07.088>, 2018.
1096



- 1097 Song, X.-H., Polissar, A. V., and Hopke, P. K.: Sources of fine particle composition in the
1098 northeastern US, *Atmos. Environ.*, 35, 5277-5286, <https://doi.org/10.1016/S1352->
1099 2310(01)00338-7, 2001.
1100
- 1101 Sorooshian, A., Varutbangkul, V., Brechtel, F. J., Ervens, B., Feingold, G., Bahreini, R.,
1102 Murphy, S. M., Holloway, J. S., Atlas, E. L., Buzorius, G., Jonsson, H., Flagan, R. C., and
1103 Seinfeld, J. H.: Oxalic acid in clear and cloudy atmospheres: Analysis of data from International
1104 Consortium for Atmospheric Research on Transport and Transformation 2004, *J. Geophys. Res.-*
1105 *Atmos.*, 111, 10.1029/2005jd006880, 2006.
1106
- 1107 Sorooshian, A., Ng, N. L., Chan, A. W. H., Feingold, G., Flagan, R. C., and Seinfeld, J. H.:
1108 Particulate organic acids and overall water-soluble aerosol composition measurements from the
1109 2006 Gulf of Mexico Atmospheric Composition and Climate Study (GoMACCS), *J. Geophys.*
1110 *Res.-Atmos.*, 112, 10.1029/2007jd008537, 2007a.
1111
- 1112 Sorooshian, A., Lu, M.-L., Brechtel, F. J., Jonsson, H., Feingold, G., Flagan, R. C., and Seinfeld,
1113 J. H.: On the Source of Organic Acid Aerosol Layers above Clouds, *Environ. Sci. Technol.*, 41,
1114 4647-4654, 10.1021/es0630442, 2007b.
1115
- 1116 Sorooshian, A., Crosbie, E., Maudlin, L. C., Youn, J.-S., Wang, Z., Shingler, T., Ortega, A. M.,
1117 Hersey, S., and Woods, R. K.: Surface and airborne measurements of organosulfur and
1118 methanesulfonate over the western United States and coastal areas, *J. Geophys. Res.-Atmos.*,
1119 120, 8535-8548, 10.1002/2015jd023822, 2015.
1120
- 1121 Stein, A. F., Draxler, R. R., Rolph, G. D., Stunder, B. J. B., Cohen, M. D., and Ngan, F.:
1122 NOAA's HYSPLIT Atmospheric Transport and Dispersion Modeling System, *B. Am. Meteorol.*
1123 *Soc.*, 96, 2059-2077, 10.1175/bams-d-14-00110.1, 2015.
1124
- 1125 Sternbeck, J., Sjödin, Å., and Andréasson, K.: Metal emissions from road traffic and the
1126 influence of resuspension—results from two tunnel studies, *Atmos. Environ.*, 36, 4735-4744,
1127 [https://doi.org/10.1016/S1352-2310\(02\)00561-7](https://doi.org/10.1016/S1352-2310(02)00561-7), 2002.
1128
- 1129 Thepnuan, D., Chantara, S., Lee, C.-T., Lin, N.-H., and Tsai, Y. I.: Molecular markers for
1130 biomass burning associated with the characterization of PM_{2.5} and component sources during
1131 dry season haze episodes in Upper South East Asia, *Sci. Total Environ.*, 658, 708-722,
1132 <https://doi.org/10.1016/j.scitotenv.2018.12.201>, 2019.
1133
- 1134 Thurston, G. D., and Spengler, J. D.: A quantitative assessment of source contributions to
1135 inhalable particulate matter pollution in metropolitan Boston, *Atmos. Environ.*, 19, 9-25,
1136 [https://doi.org/10.1016/0004-6981\(85\)90132-5](https://doi.org/10.1016/0004-6981(85)90132-5), 1985.
1137
- 1138 Vaughan, M. A., Young, S. A., Winker, D. M., Powell, K. A., Omar, A. H., Liu, Z., Hu, Y., and
1139 Hostetler, C. A.: Fully automated analysis of space-based lidar data: an overview of the
1140 CALIPSO retrieval algorithms and data products, *Proc. SPIE*, 5575,
1141 <https://doi.org/10.1117/12.572024>, 2004.
1142



- 1143 Wang, H., and Shooter, D.: Low molecular weight dicarboxylic acids in PM10 in a city with
1144 intensive solid fuel burning, *Chemosphere*, 56, 725-733,
1145 <https://doi.org/10.1016/j.chemosphere.2004.04.030>, 2004.
1146
- 1147 Wang, J., Ge, C., Yang, Z., Hyer, E. J., Reid, J. S., Chew, B.-N., Mahmud, M., Zhang, Y., and
1148 Zhang, M.: Mesoscale modeling of smoke transport over the Southeast Asian Maritime
1149 Continent: Interplay of sea breeze, trade wind, typhoon, and topography, *Atmos. Res.*, 122, 486-
1150 503, <https://doi.org/10.1016/j.atmosres.2012.05.009>, 2013.
1151
- 1152 Wang, S.-H., Tsay, S.-C., Lin, N.-H., Hsu, N. C., Bell, S. W., Li, C., Ji, Q., Jeong, M.-J.,
1153 Hansell, R. A., Welton, E. J., Holben, B. N., Sheu, G.-R., Chu, Y.-C., Chang, S.-C., Liu, J.-J.,
1154 and Chiang, W.-L.: First detailed observations of long-range transported dust over the northern
1155 South China Sea, *Atmos. Environ.*, 45, 4804-4808,
1156 <https://doi.org/10.1016/j.atmosenv.2011.04.077>, 2011.
1157
- 1158 Weber, R. J., Sullivan, A. P., Peltier, R. E., Russell, A., Yan, B., Zheng, M., de Gouw, J.,
1159 Warneke, C., Brock, C., Holloway, J. S., Atlas, E. L., and Edgerton, E.: A study of secondary
1160 organic aerosol formation in the anthropogenic-influenced southeastern United States, *J.*
1161 *Geophys. Res.-Atmos.*, 112, 10.1029/2007jd008408, 2007.
1162
- 1163 Wen, H., and Carignan, J.: Reviews on atmospheric selenium: Emissions, speciation and fate,
1164 *Atmos. Environ.*, 41, 7151-7165, <https://doi.org/10.1016/j.atmosenv.2007.07.035>, 2007.
1165
- 1166 Winker, D. M., Vaughan, M. A., Omar, A., Hu, Y., Powell, K. A., Liu, Z., Hunt, W. H., and
1167 Young, S. A.: Overview of the CALIPSO Mission and CALIOP Data Processing Algorithms, *J.*
1168 *Atmos. Ocean. Tech.*, 26, 2310-2323, 10.1175/2009jtech1281.1, 2009.
1169
- 1170 Wonaschuetz, A., Sorooshian, A., Ervens, B., Chuang, P. Y., Feingold, G., Murphy, S. M., de
1171 Gouw, J., Warneke, C., and Jonsson, H. H.: Aerosol and gas re-distribution by shallow cumulus
1172 clouds: An investigation using airborne measurements, *J. Geophys. Res.-Atmos.*, 117,
1173 10.1029/2012jd018089, 2012.
1174
- 1175 Xian, P., Reid, J. S., Atwood, S. A., Johnson, R. S., Hyer, E. J., Westphal, D. L., and Sessions,
1176 W.: Smoke aerosol transport patterns over the Maritime Continent, *Atmos. Res.*, 122, 469-485,
1177 <https://doi.org/10.1016/j.atmosres.2012.05.006>, 2013.
1178
- 1179 Xu, J., Zhang, J., Liu, J., Yi, K., Xiang, S., Hu, X., Wang, Y., Tao, S., and Ban-Weiss, G.:
1180 Influence of cloud microphysical processes on black carbon wet removal, global distributions,
1181 and radiative forcing, *Atmos. Chem. Phys.*, 19, 1587-1603, 10.5194/acp-19-1587-2019, 2019.
1182
- 1183 Yamasoe, M. A., Artaxo, P., Miguel, A. H., and Allen, A. G.: Chemical composition of aerosol
1184 particles from direct emissions of vegetation fires in the Amazon Basin: water-soluble species
1185 and trace elements, *Atmos. Environ.*, 34, 1641-1653, <https://doi.org/10.1016/S1352->
1186 2310(99)00329-5, 2000.
1187

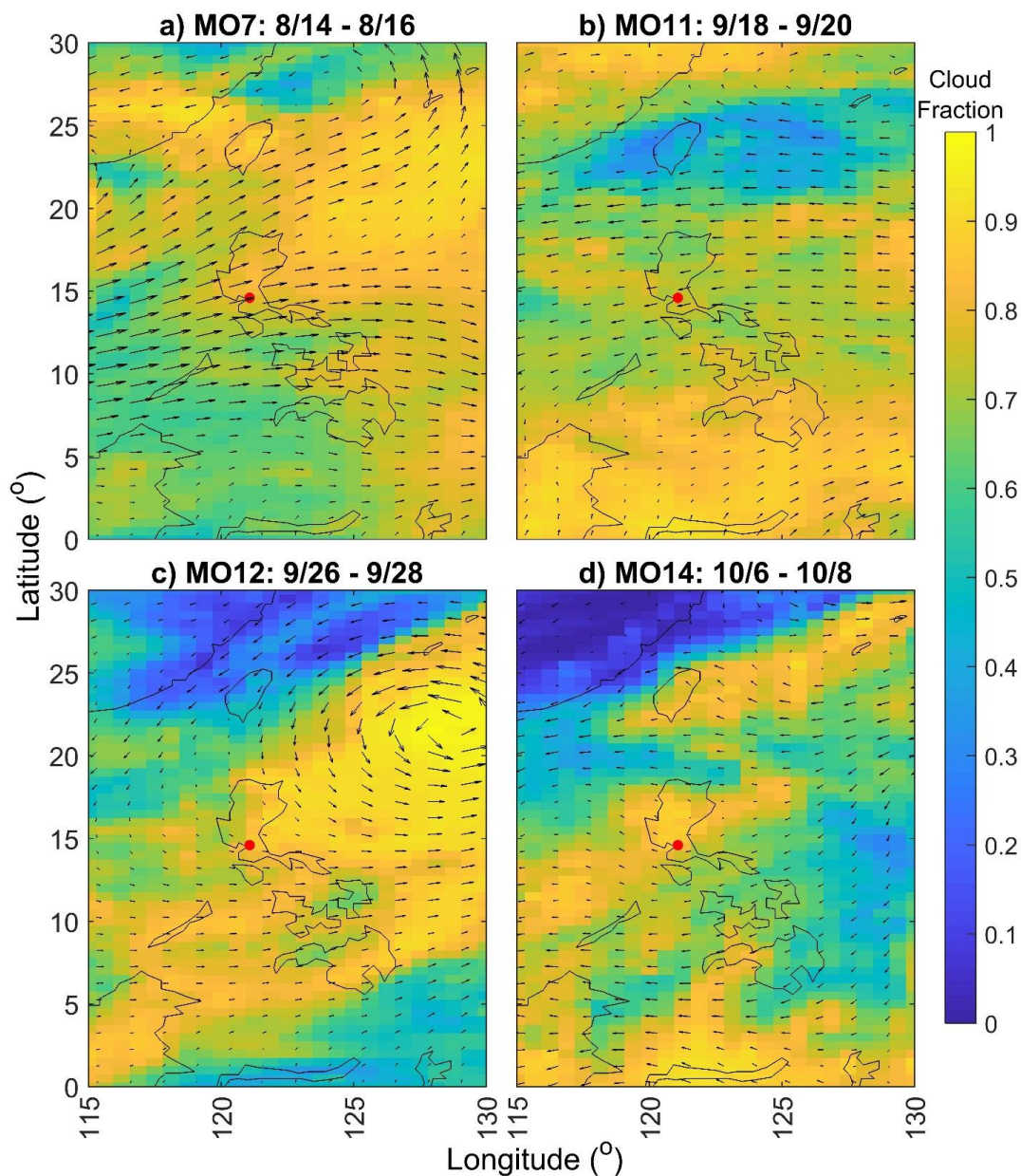


- 1188 Yan, J., Chen, L., Lin, Q., Zhao, S., and Zhang, M.: Effect of typhoon on atmospheric aerosol
1189 particle pollutants accumulation over Xiamen, China, *Chemosphere*, 159, 244-255,
1190 <https://doi.org/10.1016/j.chemosphere.2016.06.006>, 2016.
1191
- 1192 Yao, X., Fang, M., Chan, C. K., Ho, K. F., and Lee, S. C.: Characterization of dicarboxylic acids
1193 in PM_{2.5} in Hong Kong, *Atmos. Environ.*, 38, 963-970,
1194 <https://doi.org/10.1016/j.atmosenv.2003.10.048>, 2004.
1195
- 1196 Yokelson, R. J., Crounse, J. D., DeCarlo, P. F., Karl, T., Urbanski, S., Atlas, E., Campos, T.,
1197 Shinzuka, Y., Kapustin, V., Clarke, A. D., Weinheimer, A., Knapp, D. J., Montzka, D. D.,
1198 Holloway, J., Weibring, P., Flocke, F., Zheng, W., Toohey, D., Wennberg, P. O., Wiedinmyer,
1199 C., Mauldin, L., Fried, A., Richter, D., Walega, J., Jimenez, J. L., Adachi, K., Buseck, P. R.,
1200 Hall, S. R., and Shetter, R.: Emissions from biomass burning in the Yucatan, *Atmos. Chem.*
1201 *Phys.*, 9, 5785-5812, [10.5194/acp-9-5785-2009](https://doi.org/10.5194/acp-9-5785-2009), 2009.
1202
- 1203 Zhang, Y.-N., Zhang, Z.-S., Chan, C.-Y., Engling, G., Sang, X.-F., Shi, S., and Wang, X.-M.:
1204 Levoglucosan and carbonaceous species in the background aerosol of coastal southeast China:
1205 case study on transport of biomass burning smoke from the Philippines, *Environ. Sci. Pollut. R.*,
1206 19, 244-255, [10.1007/s11356-011-0548-7](https://doi.org/10.1007/s11356-011-0548-7), 2012.
1207
- 1208 Zhao, X., Wang, X., Ding, X., He, Q., Zhang, Z., Liu, T., Fu, X., Gao, B., Wang, Y., Zhang, Y.,
1209 Deng, X., and Wu, D.: Compositions and sources of organic acids in fine particles (PM_{2.5}) over
1210 the Pearl River Delta region, south China, *J. Environ. Sci.*, 26, 110-121,
1211 [https://doi.org/10.1016/S1001-0742\(13\)60386-1](https://doi.org/10.1016/S1001-0742(13)60386-1), 2014.

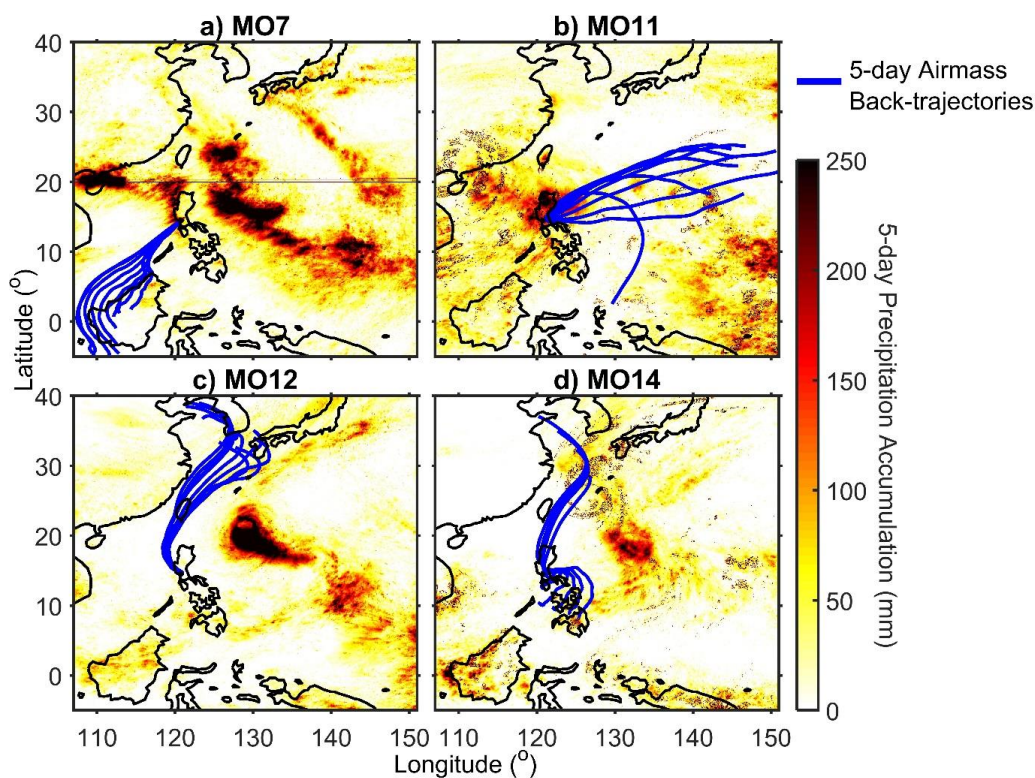


1212 **Table 1.** Description of the MOUDI sample sets from this study. Accumulated precipitation
1213 during the sample sets was found using PERSIANN-CCS for the area bounded by: 121.0199 -
1214 121.0968° E and 14.6067 - 14.6946° N.
1215

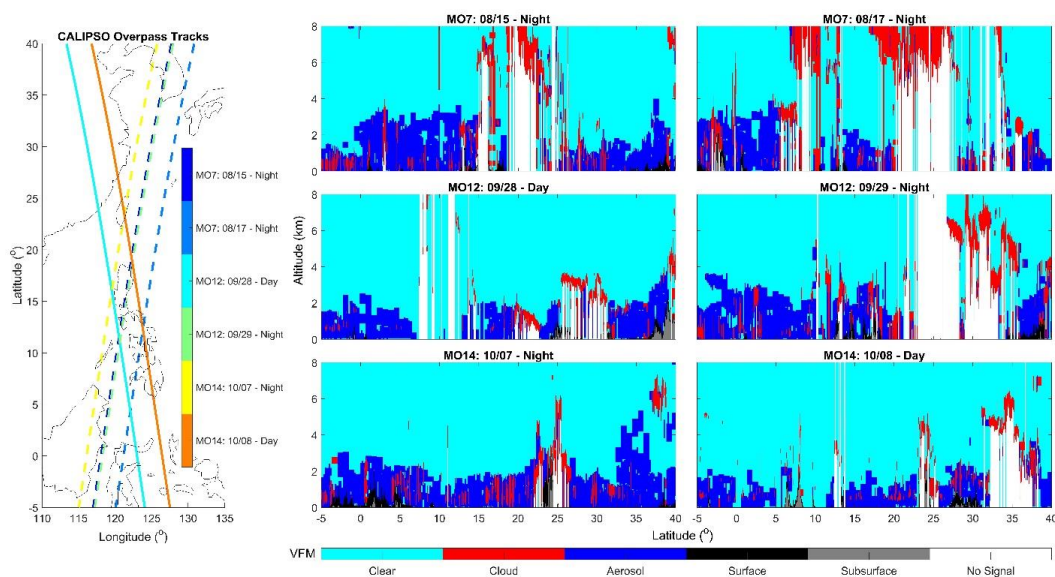
Set Name	Start Date/ Local Time	End Date/ Local Time	Total Water-Soluble Species ($\mu\text{g m}^{-3}$)	% of water- soluble mass < 1 μm	Precipitation (mm)
MO1	7/19/18 12:40 PM	7/20/18 12:43 PM	4.61	67.3%	27
MO2	7/23/18 11:29 AM	7/25/18 5:10 PM	6.52	62.1%	14
MO4	7/25/18 7:16 PM	7/30/18 6:12 PM	5.17	66.4%	35
MO5	7/30/18 7:17 PM	8/1/18 1:19 PM	9.17	64.8%	11
MO6	8/6/18 2:33 PM	8/8/18 2:38 PM	5.11	55.8%	50
MO7	8/14/18 1:59 PM	8/16/18 2:04 PM	13.70	60.3%	3
MO8	8/22/18 1:46 PM	8/24/18 1:53 PM	12.73	71.6%	10
MO9	9/1/18 5:00 AM	9/3/18 5:05 AM	6.23	76.7%	64
MO10	9/10/18 2:42 PM	9/12/18 3:02 PM	6.36	79.5%	20
MO11	9/18/18 2:12 PM	9/20/18 2:24 PM	2.70	47.3%	26
MO12	9/26/18 1:53 PM	9/28/18 1:53 PM	13.49	59.9%	1
MO14	10/6/18 5:00 AM	10/8/18 5:05 AM	16.55	78.4%	0



1216
1217 **Figure 1.** MERRA-2 data for 850 hPa wind vectors and total cloud fraction averaged over the
1218 sample set duration for a) MO7 (8/14 – 8/16), b) MO11 (9/18 – 9/20), c) MO12 (9/26 – 9/28),
1219 and d) MO14 (10/6 – 10/8). The location of the Manila Observatory is indicated by the red
1220 circle. (Note that 850 hPa wind vectors are also averaged to increase grid spacing and improve
1221 figure readability.)

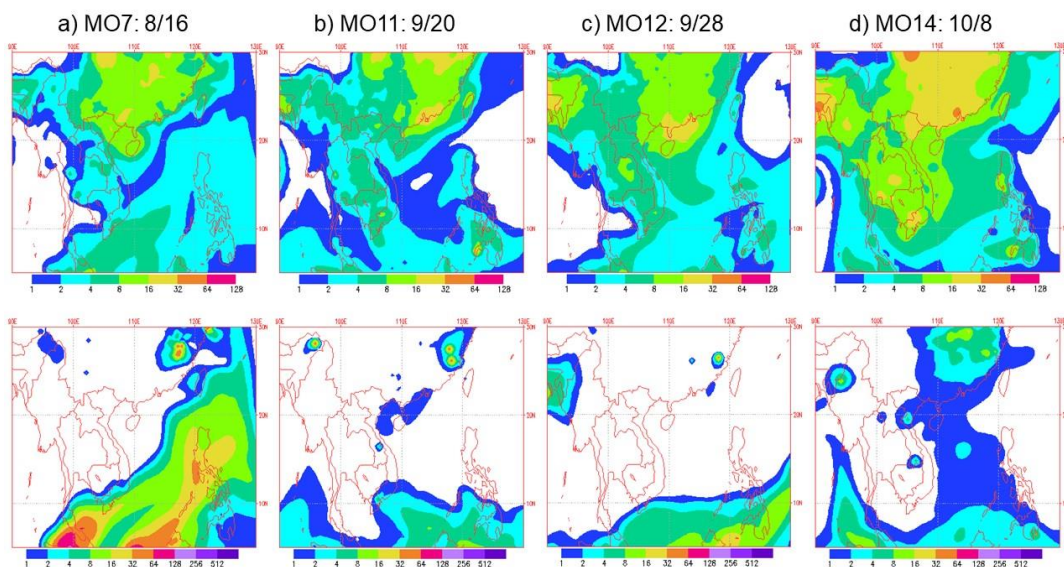


1222
1223 **Figure 2.** Rainfall accumulation, extending from 5 days before the midpoint of each sample set
1224 until the midpoint of each sample set, from PERSIAN-CCS for a) MO7, b) MO11, c) MO12, and
1225 d) MO14. In blue are the 5-day air mass back-trajectories terminating at the MOUDI inlet at MO
1226 (~85 m above sea level) every 6 h during each of the sample study periods. Note that the
1227 maximum precipitation accumulation in the region shown during the study periods was 955 mm;
1228 however, for figure readability, the scale was reduced to 0-250 mm.

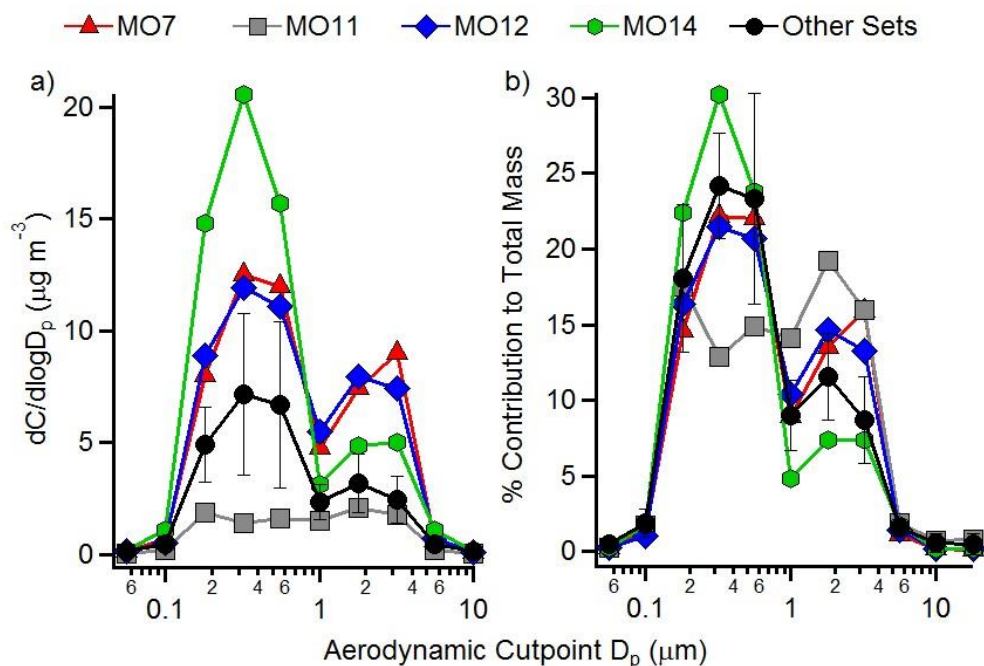


1229
1230
1231
1232
1233
1234
1235

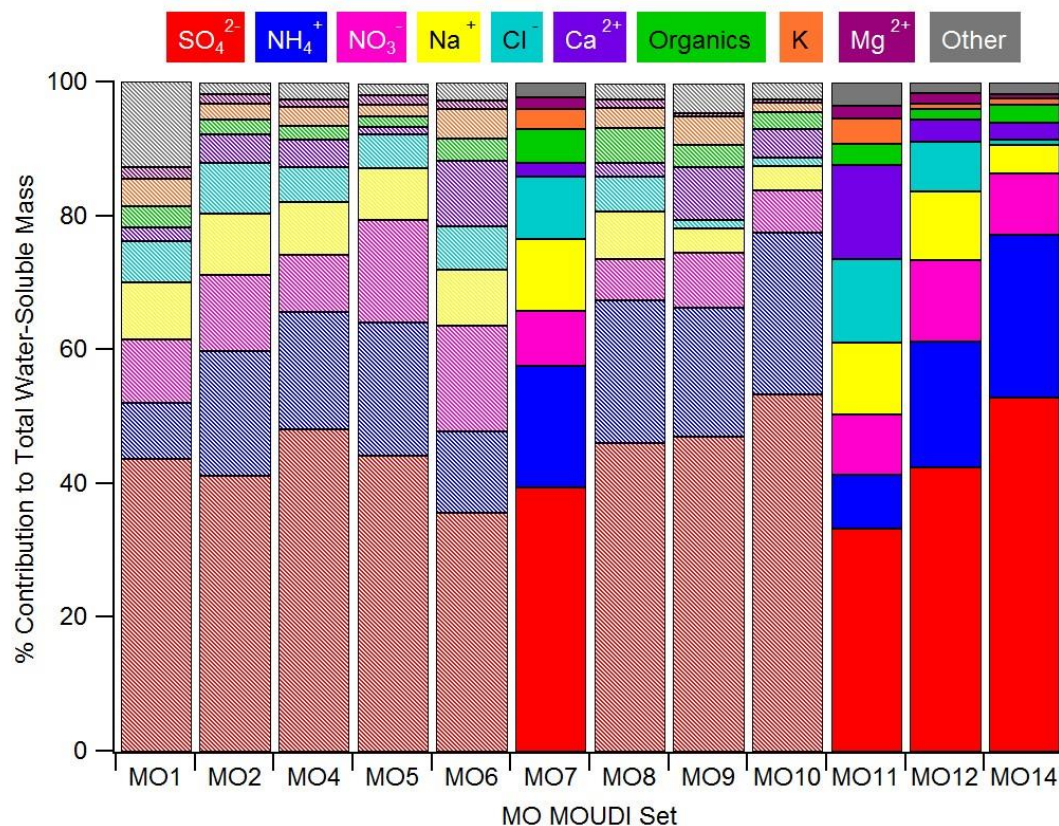
Figure 3. CALIOP Vertical Feature Mask (VFM) for overpasses during or following MO7, MO12, and MO14. For the CALIPSO satellite overpass tracks, the dashed lines correspond to the nighttime profiles and solid lines are for daytime. Note that nighttime overpasses correspond to early morning times before sunrise for the listed days and daytime overpasses occurred during early afternoon.



1236
1237 **Figure 4.** NAAPS model snapshots corresponding to conditions at the stop time of sample sets a)
1238 MO7, b) MO11, and c) MO12 and d) 3 h after the sample stop time for MO14. The top row of
1239 figures is anthropogenic and biogenic fine aerosol (ABF) surface concentration ($\mu\text{g m}^{-3}$), while
1240 the bottom row is biomass burning smoke surface concentration ($\mu\text{g m}^{-3}$).

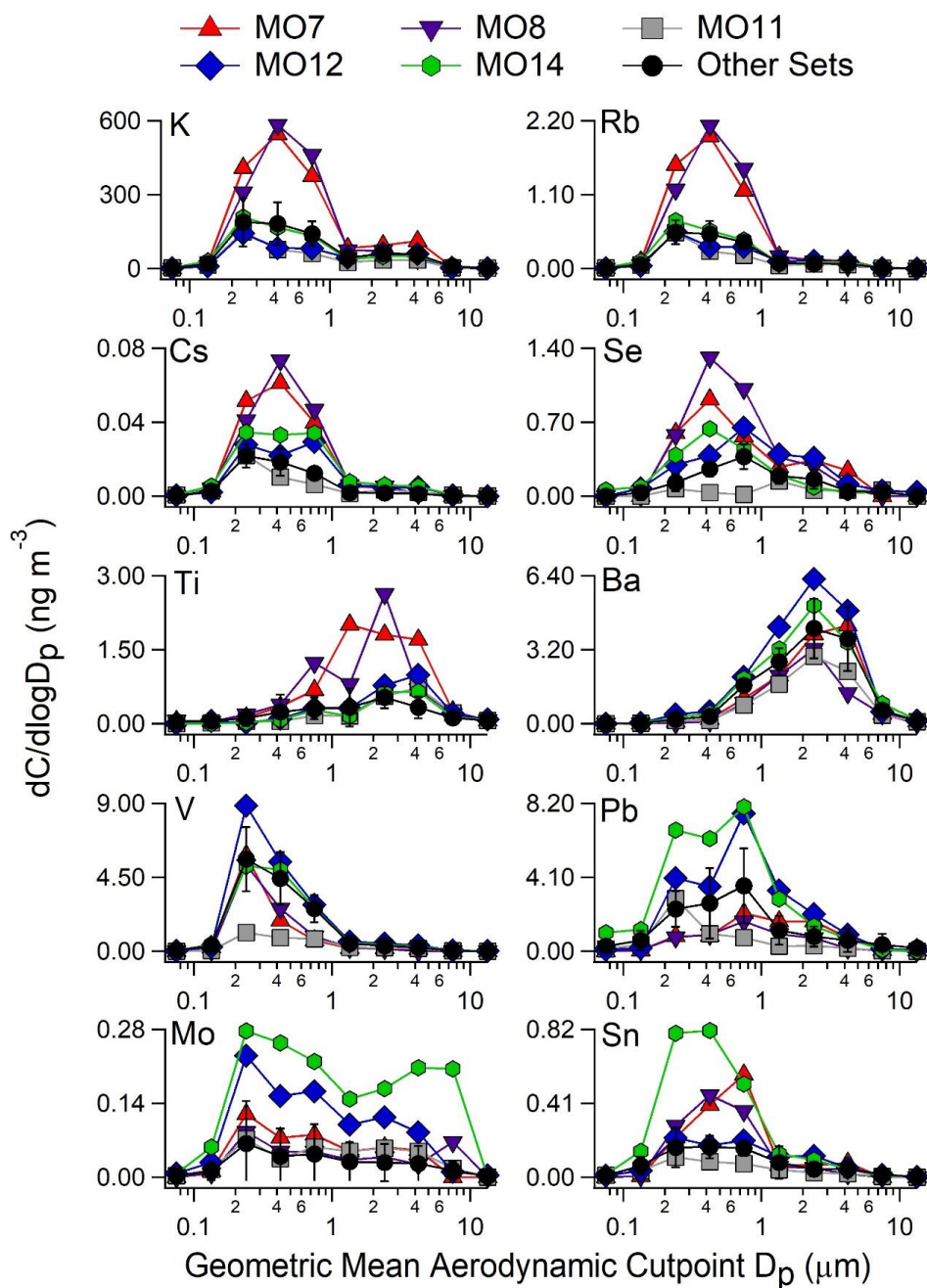


1241
1242 **Figure 5.** a) Mass size distributions for total water-soluble mass ($C =$ sum of mass
1243 concentrations for water-soluble species) and b) percent contribution of each size range to the
1244 total water-soluble mass for the three MOUDI sets with the highest aerosol mass concentrations
1245 (MO7, MO12, and MO14), the set with the lowest concentration (MO11), and the average (\pm one
1246 standard deviation error bars) for the remaining eight sets.
1247



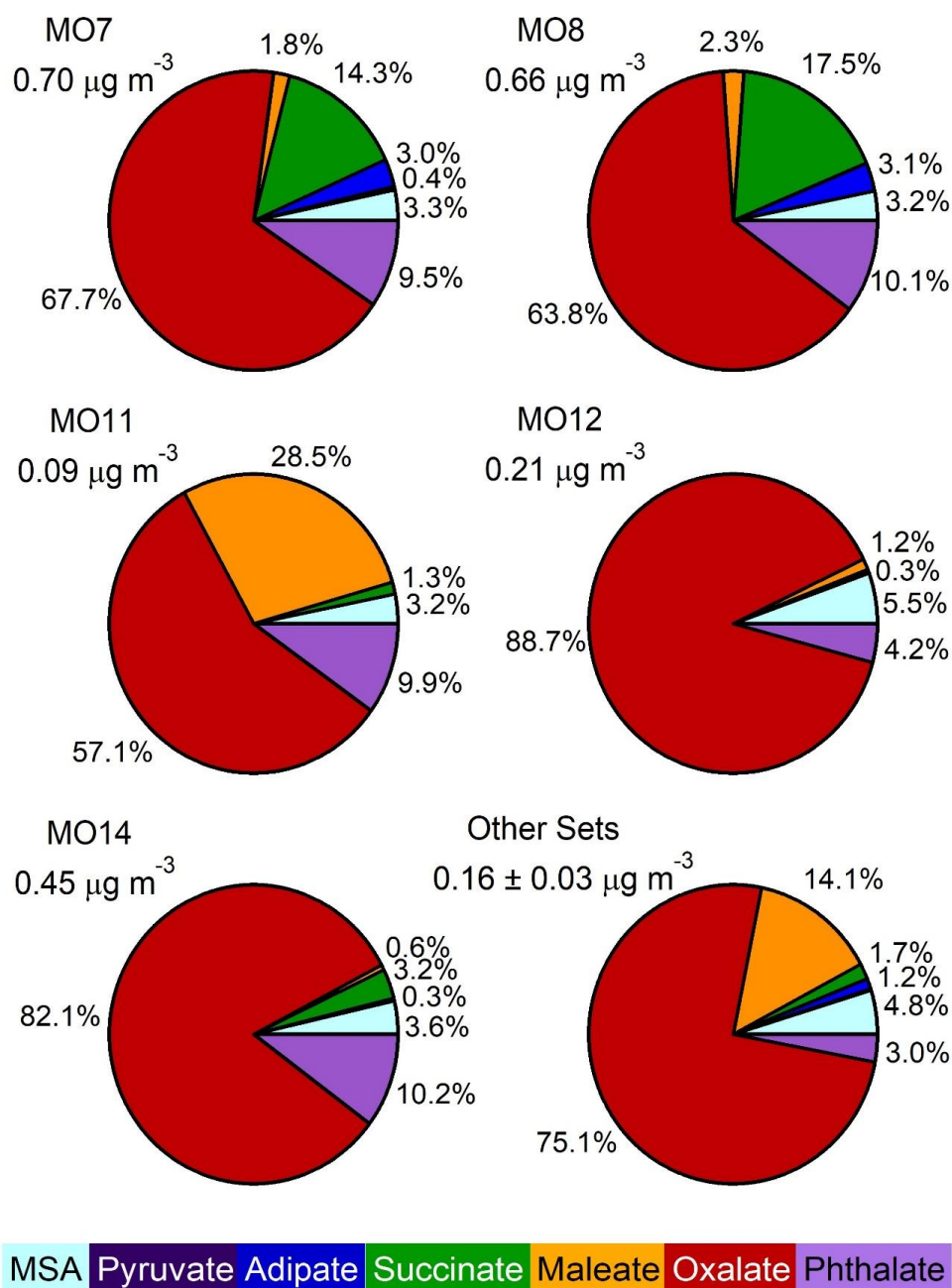
1248
1249
1250
1251
1252
1253

Figure 6. Percent contribution of various species to the total water-soluble mass concentration for each of the 12 sample sets. The sample sets with the three highest aerosol concentrations (MO7, MO12, and MO14) and the lowest aerosol concentration (MO11) are shown as solid bars while all other sample sets are stripes. The “organics” category contains the sum of methanesulfonate (MSA), pyruvate, adipate, succinate, maleate, oxalate, and phthalate.



1254
1255
1256
1257
1258

Figure 7. Selected elements that showed elevated concentrations during at least one of the highest aerosol events (MO7, MO8, MO12, or MO14). The concentrations from the lowest aerosol event (MO11) are also shown. The “other sets” category displays the average (\pm one standard deviation) for the remaining seven sets.



1259
 1260
 1261
 1262
 1263
 1264

Figure 8. Pie charts showing the fraction of species contributing to the measured water-soluble organic aerosol. Below each pie chart title is the sum of the water-soluble organic species measured, with the “other sets” chart showing the average \pm one standard deviation for the remaining sets. Acronyms: Methanesulfonate (MSA)